B.ŞENEL

ATILIM UNIVERSITY 2021

TOPOLOGY OPTIMIZATION OF A SANDWICH STRUCTURAL COMPONENT AGAINST HIGH IMPULSE LOADINGS

THE GRADUATE SCHOOL OF NATURAL AND APPLIED SCIENCES
OF
ATILIM UNIVERSITY

BARKIN ŞENEL

A MASTER OF SCIENCE THESIS
IN
THE DEPARTMENT OF MECHANICAL ENGINEERING

JUNE 2021

TOPOLOGY OPTIMIZATION OF A SANDWICH STRUCTURAL COMPONENT AGAINST HIGH IMPULSE LOADINGS

A THESIS SUBMITTED TO
THE GRADUATE SCHOOL OF NATURAL AND APPLIED SCIENCES
OF
ATILIM UNIVERSITY

BY

BARKIN ŞENEL

IN PARTIAL FULFILLMENT OF THE REQUIREMENTS
FOR
THE DEGREE OF MASTER OF SCIENCE
IN
MECHANICAL ENGINEERING

JUNE 2021

Approval of the Graduate School of Natural and Applied Sciences, Atilim University.

Prof. Dr. Ender Keskinkılıç
Director

I certify that this thesis satisfies all the requirements as a thesis for the degree of **Master of Science in Mechanical Engineering Department, Atilim University**.

Prof. Dr. S. Engin Kılıç
Head of Department

This is to certify that we have read the thesis TOPOLOGY OPTIMIZATION OF A SANDWICH STRUCTURAL COMPONENT AGAINST HIGH IMPULSE LOADINGS submitted by BARKIN ŞENEL and that in our opinion it is fully adequate, in scope and quality, as a thesis for the degree of Master of Science.

Asst.Prof.Dr. Besim Baranoğlu
Co-Supervisor

Assoc.Prof. Dr. Özgür Aslan
Supervisor

Examining Committee Members:

Prof. Dr. A. Hakan Argeşo
Aerospace Engineering, Atilim University

Assoc. Prof. Dr. Özgür Aslan
Mechanical Engineering,Atilim University

Assoc. Prof. Dr. Ebru Saraloğlu Güler
Mechanical Engineering, Baskent University

Date: June 24, 2021

I declare and guarantee that all data, knowledge and information in this document has been obtained, processed and presented in accordance with academic rules and ethical conduct. Based on these rules and conduct, I have fully cited and referenced all material and results that are not original to this work.

Name, Last Name : BARKIN ŞENEL

Signature :

ABSTRACT

TOPOLOGY OPTIMIZATION OF A SANDWICH STRUCTURAL COMPONENT AGAINST HIGH IMPULSE LOADINGS

Şenel, Barkın

M.S., Department of Mechanical Engineering

Supervisor : Assoc.Prof. Dr. Özgür Aslan

Co-Supervisor : Asst.Prof.Dr. Besim Baranoğlu

June 2021, 49 pages

Sandwich structures are used in many areas today due to their lightness, economy and durability. Application in armoured military vehicles is one of these areas. According to previous studies in the literature, sandwich structures provide a great advantage over monolith structures. Today, researchers try to develop sandwich structures in terms of material or topology optimization to further increase this advantage. Numerical analysis trials applied before experimental studies, on the other hand, help this development in terms of time and cost. In this thesis, different core geometry types selected are modelled in the SolidWorks package program. Then, the analyses were made in the ABAQUS/Explicit finite element program. Initially, analyses were performed under fixed parameters for evaluation and comparison purposes only. According to the results, the material parameters were determined according to the material parameters to be used in production and the analyses continued in this way. However, in this study, no material optimization was made, only the topology was focused. In addition, while the geometries are modelled, it is aimed to determine the selected geometry types in a way that will not cause problems in terms of production. With these determined parameters and analyses, an optimum core geometry has been proposed, which is also easy in terms of production.

Keywords: sandwich structure, impulse loadings, numerical analysis, optimization

ÖZ

YÜKSEK DARBELİ YÜKLEMELERE KARŞI SANDVİÇ YAPISAL BİLEŞENİN TOPOLOJİ OPTİMİZASYONU

Şenel, Barkın

Yüksek Lisans, Makine Mühendisliği

Tez Yöneticisi : Doç. Dr. Özgür Aslan

Ortak Tez Yöneticisi : Dr. Öğr. Üyesi Besim Baranoğlu

Haziran 2021, 49 sayfa

Sandviç yapılar, hafif, ekonomik ve dayanıklı olmasından dolayı günümüzde bir çok alanda kullanılmaktadır. Zırhlı askeri araçlardaki uygulamalar da bu alanlardan biridir. Literatürde daha önceden yapılan çalışmalara göre, sandviç yapılar, monolit yapılara karşı büyük avantaj sağlamaktadır. Günümüzde araştırmacılar, bu avantajı artırmak için malzeme veya topoloji optimizasyonu açısından sandviç yapıları geliştirmek için çalışmaktadır. Deneysel çalışmalardan önce uygulanan nümerik analiz denemeleri ise bu geliştirmeye zaman ve maliyet açısından yardımcı olmaktadır. Bu tez çalışmasında, seçilen farklı çekirdek geometri tipleri SolidWorks paket programında modellenmiştir. Daha sonra ise ABAQUS/ Explicit sonlu elemanlar programında analizleri yapılmıştır. Başlangıçta, sadece değerlendirme ve karşılaştırma amacıyla sabit parametreler altında analizler gerçekleştirilmiştir. Çıkan sonuçlara göre malzeme parametreleri, üretimde kullanılacak malzeme parametrelerine göre belirlenip analizler yapılmıştır. Fakat bu çalışmada, malzeme optimizasyonu yapılmamış, sadece topolojiye odaklanılmıştır. Ayrıca geometriler modellenirken, seçilen geometri tiplerinin üretim açısından sorun çıkarmayacak şekilde belirlenmesi amaçlanmıştır. Belirlenen bu parametreler ve analiz sonuçları ile, üretim açısından da kolay olmak üzere optimum bir çekirdek geometrisi

önerilmiştir.

Anahtar Kelimeler: sandviç yapı, darbe yüklemeleri, sayısal analiz, optimizasyon

To My Family

ACKNOWLEDGMENTS

First and foremost, I would like to thank my supervisor, Assoc. Prof. Dr. Özgür Aslan, whose guidance and advice was invaluable.

I would like to devote my sincere thanks to Asst. Prof. Dr. Besim Baranoğlu for his valuable feedbacks of this thesis.

I would like to gratefully acknowledge the support of FNSS Defence System; especially special thanks to Barış Çetin for his support and guidance during this research.

I shall also thank to the support and great love of my family, my mother, Fügen Şenel; and my father, Ümit Şenel. They kept me going on and this study would not have been possible without their input.

Furthermore, I am thankful to the researchers of CSE LAB whom Gamze Çakır Kabakcı and Ferit Sait. My appreciation goes out to them for their encouragement and support all through my studies. Besides, I am very thankful for the support and friendship of Gizem Nur Bulanık Durmuş, İrem Bulanık Özdemir and Ethem Teke.

Finally, I also would like to thank to Deniz Şahin who supported me with her patience and love. This study would not have been possible without her.

TABLE OF CONTENTS

LIST OF TABLES

TABLES

LIST OF FIGURES

FIGURES

CHAPTER 1

INTRODUCTION

1.1 General Overview

Today, the defence industry is becoming increasingly important due to the increasing terrorist attacks and geopolitical reasons and this situation increase the need of using more durable products. Especially, developing countries like our country need more improvement in this area to reduce foreign dependency. Considering over truths, Turkey must be able to plan and make its national vehicle that can be utilized under the command of the Turkish security forces. Many programs, both by the government and the private sector, have been implemented in recent years to ensure national security investigations (Fig. 1.1)[1]. As a result, foreign dependency has decreased and the rate of domestic product use in the defence industry has been also increased.

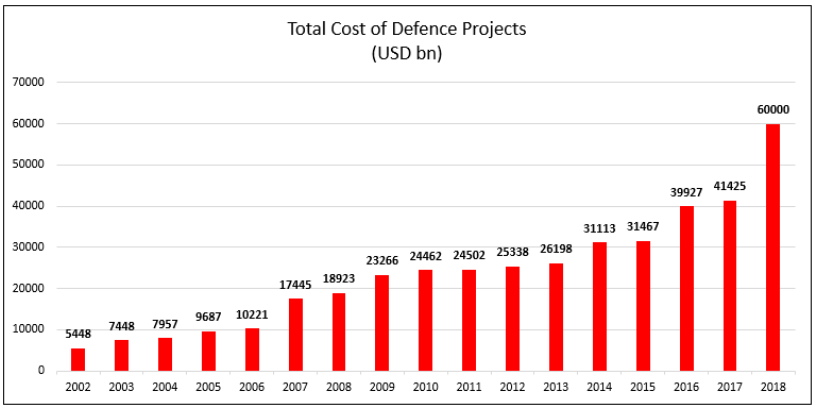

Figure 1.1: Graph of the Number of Projects by Years

In particular, the need for locally produced armoured land vehicles is increased, and

accordingly studies and projects on this subject have gained momentum. The products that come out of these projects have been added to the inventory in recent years and the product variety in the inventory has also increased (Fig. 1.2)[2]. Before these products are delivered, they are expected to be successful in various tests and meet the general standards. One of the major expectations of armed forces vehicles is the survival of the passengers during assaults. In order to accomplish this purpose, cars are usually fitted with heavy steel armour. However, even if this provides protection, it also makes the vehicle heavier. The safety of the passengers is also contingent on the mobility of the vehicles in a hot war environment. A lighter armoured carrier can transport personnel to the safe zone, as it can move faster than a heavier vehicle with the same level of damage. Therefore, it is an primarily required that the vehicle is lighter and faster, as well as providing necessary.

(a) PARS III 6x6 (b) ACV-AD (c) ACV-19

Figure 1.2: Different Armoured Vehicle Products

Sandwich structures are widely used in many engineering sectors, including automotive manufacture (car, armour vehicle and plane). Sandwich panels are classified into three types: (1) natural based of fiber (2) synthetical based of fiber, and (3) metal-based [3]. Because of their high stiffness-to-weight ratio, high strength-to-weight ratio and high energy absorption potential,, the initial design geometry used in lightweight armour construction has been proposed as sandwich structures. The framework of a sandwich structure consists of a light, dense core sandwiched between thin, rigid face sheets. Sandwiches have high flexural stability with a thicker and lighter core between face sheets, and better energy absorption can be assured by sandwich structures by the use of collapsible structures as core materials. Compared to monolith panels, sandwich panels have better strength-to-weight ratios. As a result, they can support comparable loads with less structural material, which can lead to lower material purchasing and transportation costs. Sandwich structures are a cost-effective

option because their core materials are less expensive than other composite reinforcement materials. Additionally, their inherent durability lowers their maintenance costs [4][5][6].

Previous studies have shown that sandwich structures used as base plates in this type of armoured vehicles provide better strength than monolithic structures and recent research indicates that incorporating a sandwich structure into a vehicle's body panel by enhancing the structure with multi-layered plates rather than a single monolith structure can decrease the overall weight of the vehicle by at least 30 % while maintaining structural integrity and increasing the limit of ballistic of that structure [7][8][9][10]. These studies show that the energy absorption capacity of the sandwich structure is determined by the core geometry and the strength of the material used for this structure. A variety of micro-architectured materials have been produced in the past years for use as the cores of sandwich structures or panels. When the important studies on core geometry are examined [11], it is observed that the important differences in energy absorption point observed between monolithic structures and sandwich structures as energy absorption characteristics are also found in the core geometries of sandwich structures, and the maximum deflection values measured in plates and deflection character are mainly dependent on the core geometry of sandwich plates.

In this thesis, finite element analysis analysis of the sandwich structure with 4 different core geometries with under blast loads, were performed by the finite element method with ABAQUS / Explicit package program. Then the behaviours of core geometries and whole structures during and after explosion were compared. Afterwards, considering the ease of production, the most suitable structure for explosion was proposed.

1.2 Literature Review

Many studies with finite element modeling in the literature say that solid plate performs worse than sandwich structure with different core geometries (triangular, folded and honeycomb)[11][12][13][14]

According to Hutchinson and Xue, the triangular, corrugated and square core geometries, most commonly used as a sandwich structure, can withstand explosions larger

than a monolithic plate of equal mass[7]. In this study, it is shown the square and folded core structure performs better than the triangular core structure, although the different thicknesses of the lower and upper plates and the exact optimizations regarding the geometry are not considered. Furthermore , Dharmasena et al. analysed three level of impulse load on the square core sandwich panel and solid plates with same weight per unit area and although there was a front face bending and cell wall buckling, and this buckling increased as the impulse increased, they proved that the back face deflections of honeycomb sandwich panels are lower than those of solid plates of equal mass [19].

According to studies in the literature, researchers focused on design parameters such as the thickness of the core structure, density of core and panel thickness in sandwich structures[23][24][25][26].On the other hand, according to Xue and Hutchinson square honeycombs or grid shape are also useful as cores for all-metal sandwich plates because they combine strong stiffness and strength in out-of-plane shear and in-plane stretch with excellent crushing strength and energy absorption [20].

Also according to Fleck and Deshpande studied that the blast resistance of sandwich beams has been studied using a modelling technique. This technique is based on three different phases. First stage is the fluid-structure interaction during the explosion. During phase II cores deformed and the velocity of the bottom panel and cores balanced respectively. The structure is brought to a halt by plastic twisting and stretching in phase III [16].

Deshpande and Fleck, also demonstrated that the strain hardening capability of the core has minimal impact on the average through-thickness compressive strain produced within the core for ratio of core mass to face surface mass. As a result, modelling the core as an ideal plastic-locking solid is sufficient and also according to them the momentum transmitted through sandwich plates is way smaller than that transmitted into a monolithic plate of the same mass [15].

1.3 Assumptions

In these analyses, all sandwich geometries have the same material, the same boundary conditions and the same stand of distance were determined for the comparison.

1.4 Limitations

This study has limits on weight per unit area, maximum deflection and manufacturability. The geometry created should not exceed 200 kg per unit area and the maximum deflection should be 300 mm. Another limit condition is the availability of the armour steel material to be used in the proposed sandwich structure. Moreover, the thickness ratio used for spot welding the upper and lower plates to the core structure is generally three to one.

1.5 The Aim

In this study, it is aimed to minimize the damage induced to the personnel inside the vehicle due to the absorption of blast energy thanks to the base plate and core geometry of the sandwich structure at the moment of explosion of armoured vehicles. In addition, the sandwich structure is intended to provide the required level of protection such as STANAG 4569 [22] and AEP-55 [21]. In this regard, the main purpose is to analyse the geometries sent by FNSS Defence System, under constant conditions and to determine and recommend the optimum geometry according to the results of the analysis.

CHAPTER 2

THEORY IN 1-D

This section is devoted to provide a comprehensive perspective on the development of the model to be created for the finite element analysis. In particular, the sandwich structure geometry is modelled as to behave as Johnson-Cook material and ConWep explosion models will be implemented. In general, a comprehensive literature search was conducted. And also, the theory part necessary for the preparation of the finite element model is examined. In the first part, the theory of the behaviour of the sandwich structure under explosion is examined.

2.1 Analytical Models for the Sandwich Structures Under Blast

According to Taylor [29], the structural reaction of sandwich systems is divided into three stages: first is the one-dimensional fluid structure interaction problem during the explosion case, which results in a uniform velocity being forced on the exterior face surface; second is the phase of core crush, during which the velocities of the panels and core equalize by momentum transfer; the third stage is the deceleration process, which involves plastic bending and stretching to bring the beam to a halt[16]. This calculation is used to determine the transverse displacement of chosen sandwich panel as a function of blast loading magnitude. Over the last century, the fundamental features of an explosion's shock wave have been thoroughly established by a mix of detailed large-scale tests and modeling. Cole[30] and Swisdak[31] give useful descriptions of the key phenomena, which are briefly summarized here in support of the current investigation.

2.1.1 Stage I: Fluid-Structure Interaction

Consider the simplistic idealization of a plane wave striking naturally and evenly on an infinite sandwich structure. The time scale of the explosion is relatively quick for the front face of a sandwich structures to function as a solid plate of mass per unit area m_f for most realistic geometries and blast cases. In this section, Taylor's one-dimensional analysis is used and studied an incoming wave in a fluid with density ρ_w and a steady velocity c_w moving in the direction of increasing x determined vertical to the sandwich panel. The source point is set at the sandwich panel's top face, and the face's transvestic deflection is shown as w(t) in terms of time, t. The pressure for the initial wave can then be calculated as follows:

$$p_I(x,t) = p_0 e^{-(t-x/c_w)/\theta} \tag{2.1}$$

where θ is time constant. Using the standard definition of an exponentially shaped blast wave with a constant value of time t. The peak pressure p_o is usually in the region of 10–100 MPa, far above the sandwich plate's static failure stress. The reflected wave would seen if the front face were static and fixed in emptiness.

$$p_{r1}(x,t) = p_o e^{-(t-x/c_w)/\theta} \tag{2.2}$$

This term refers to the reflection of the wave moving in the x direction. However, the front face not fixed, it is increases the pace a static body with a mass per unit area(m_f) and moves with a $\dot{w}$(t). As a result, the flow affecting the front face has a common velocity $\dot{w}$(t) and reduction wave p_{r2}.

$$p_{r2}(x,t) = -\rho_w c_w \dot{w}\left(t + \frac{x}{c_w}\right) \tag{2.3}$$

is emitted from the top face. As a result, the total pressure $p(x,t)$ caused by reached and reflected waves is

$$p(x,t) = p_1 + p_{r1} + p_{r2} = p_0[e^{-(t-x/c_w)/\theta} + e^{-(t-x/c_w)/\theta}] - \rho_w c_w \dot{w}\left(t + \frac{x}{c_w}\right) \tag{2.4}$$

By applying initial conditions such as $\dot{w} = 0$, a simpler net pressure equation can be obtained. Additionally giving the governing ordinary differential equation for panel move to the front face of sandwich structure as

$$m_f \ddot{w} + \rho_w c_w \dot{w} = 2p_0 e^{-t/\theta} \tag{2.5}$$

Taylor also demonstrated the dynamic response applied by structural support limits to the front face by adding the kw term to the Equation 2.5. And also, according to Taylor, I is the highest achievable impulse provided by

$$I = \int_0^\infty 2p_0 e^{-t/\theta} dt = 2p_0\theta \tag{2.6}$$

But in the case of a stationary static front face is this maximal impulse realized.

In conclusion, the stage I of the analysis consists of the incoming (and reflected) first shock wave accelerating the front face to a velocity v_0. During this first step, the sandwich beam's core and back face stay constant. The acquired velocity of a front face with an impulse of magnitude $10^3\ Nsm^{-2}$ in air is approximately v_0 is equal $13m/s$ for the air blast, if the thickness of metal is equal to 10 mm. Also, the first stage can be neglected depending on the core thickness used in sandwich structure.

2.1.2 Stage II: Cores Crush

The core geometry is expected to be compressed by the advancing exterior face panel during the phase II of the motion, and as a result, the exterior face panel is slowed down by the core geometry while the core and the back face of the sandwich structure are step up. For the sake of clarity, assume a one-dimensional slice through the thickness of the sandwich structure and ignore the momentum decrease caused by the impulse given by the supports. The reason for this calculation is that the time span of this step is much shorter than the average structural reaction time of the structure. And also,the sandwich structure's ensuing retardation is caused by plastic bending and expanding in next phase of the move. The core geometry is regarded as a hard, typically plastically crushable solid with a nominal crush strength σ_{ny} up to a nominal

densification strain ϵ_D. It is claimed that the core is durable after densification has occurred.

At the end of this section, the core compression strain ϵ_c and the common velocity v_f at the surface and the core are used to evaluate. These values ϵ_c and v_f are sufficient to calculate the deviation in the next stage. Moreover, in order to obtain extra information on the core crush phase, such as the period for core crush T_c, a one-dimensional plastic shock wave analysis is needed.

This is how the conservation of momentum in the second stage is determined

$$(2m_f + \rho_c c)v_f = m_f v_0 \tag{2.7}$$

In addition, compression strain ϵ_c can also be written as

$$\epsilon_c = \frac{\epsilon_D}{2}\frac{\hat{\rho}+1}{\hat{\rho}+2}\hat{I}^2 \tag{2.8}$$

where $\hat{\rho}$=ρ_cc/m_f. The impulse given by the support reactions during the core compression process is ignored in the Stage II study. This theory fails as short structures are exposed to massive impulses.

This approach supposes that the core compresses evenly through its thickness under continuous tension. In fact, the core can compress randomly as a result of buckling of elements within the core and inertial effects. To determine the progress of strain within the core, a plastic shock wave analysis can be fulfilled. Suppose that following the effect of the front face layer on the core, a plastic shock wave of velocity c_{pl} travels into the core and after a time t, the shock wave has moved by a distance X. The velocity v_u of the shock wave, the undeformed core, and the rear face of the sandwich beam, while downstream of the shock wave, the core has compressed to the densification strain ϵ_D and shares the velocity v_d with the front face. Shock wave transmission behaviour can be estimated.

From conservation of momentum such as;

$$[m_f + \rho_c(c - X)]v_u + [m_f + \rho_c X]v_d = m_f v_0 \tag{2.9}$$

And conservation of energy

$$\frac{1}{2}m_f v_0^2 = \frac{1}{2}[m_f + \rho_c(c - X)]v_u^2 + \frac{1}{2}[m_f + \rho_c X]v_d^2 + \sigma_{nY}\epsilon_D X \tag{2.10}$$

Moreover front face panel displaces by

$$s_d = v_0 - t - \frac{\sigma_{nY}}{2m_f}t^2 \tag{2.11}$$

And the rear face panel displaces by

$$s_u = \frac{\sigma_{nY}}{2m_f}t^2 \tag{2.12}$$

Also we can write the non-dimensional core compression time which is $\hat{T}_c$, in terms of non-dimensional impulse $\hat{I}$ move to structure as below

$$\hat{T}_c \equiv \frac{T_c v_0}{\epsilon_D c} = \frac{\hat{I}}{2}[\hat{I} - \sqrt{\hat{I}^2 - 4}] \tag{2.13}$$

According to Qiu et al's finite element calculations, the additional mechanism is tensile stretching of the exterior face near the supports, as well as extra crushing of the core under rapidly rising stress[17].

2.1.3 Stage III: Dynamic Structural Response of Sandwich Structure

The core, top and bottom panel of sandwich structures have a constant velocity v_f at the end of stage II as mentioned above. The last stage of sandwich reaction consists of dissipating the kinetic energy gained by the structures between phase I and II by a combination of beam bending and spreading. The structure is assumed to have a length $2L$, mass per unit length m, and an initial velocity v_f. Especially, Jones [27] has studied large deflection solution for large v_f and Symmonds has studied small

deflection [28]. The beam's active plastic straining is caused by a combination of plastic bending and stretching, with shear yielding being ignored. Outcome longitudinal force N_0 and the bending moment M_0 have been described for the structure. In the dynamic analysis, it is assumed that displacements occur only in a direction transverse to the original axis of the beam and thus stretching is a result of only transverse displacements.

The move of the structure can be divided into two stages, as in Symmonds' small deflection research. The central part of the beam moves at the original velocity v_f in step I, while parts of length ξ at either end rotate around the supports. As a result, time intervals of curvature exist only at the ends of the rotating sectors, while axial straining occurs over the entire length of the rotating sectors. The displacement of the mid-point w_1 can be written like this

$$w_1 = v_f T_1 = \frac{M_0}{N_0}\left[\sqrt{4 + \frac{mL^2 v_f^2 N_0}{3M_O^2}} - 2\right] \tag{2.14}$$

At the next stage, the moment varies from $-M_o$ at the beam end to $+M_o$ in the middle of the length. The midspan of the structure's maximum deflection is

$$w = \sqrt{\frac{v_f^2}{\omega^2} + \left(\frac{2M_0}{N_0} + w_1\right)^2} - \frac{2M_0}{N_0} \tag{2.15}$$

Also, the maximum deflection of back and top panel of sandwich structure at the midspan can be shown non-dimensionally as

$$\overline{w} = \frac{w}{L} = \frac{\alpha_2}{2}\left[\sqrt{1 + \frac{8\overline{I}^2 \zeta^2 \alpha_3}{3\alpha_1 \alpha_2}} - 1\right] \tag{2.16}$$

and

$$\overline{w_0} = \overline{w} + \overline{c} \tag{2.17}$$

respectively. The deflection of the sandwich structure's interior face is owing only to

third phase of the deformation cycle, while the deflection of the exterior face is the total amount of the deflections in stage III and the deflection due to core compression in second phase. The tensile strain ϵ_m in the panel is written as

$$\epsilon_m = \frac{1}{2}\left(\frac{w}{L}\right) \tag{2.18}$$

By adjusting this strain ϵ_m to equal the tensile ductility ϵ_f of the face sheet steel, an expression for the absolute non-dimensional impulse I_c that the sandwich structure can withstand with no tensile failure of the face sheets is achieved and sum of Equation 2.16 and Equation 2.18 gives

$$\overline{I_c} = \frac{I}{\zeta}\sqrt{\frac{3\alpha_1\alpha_2}{8\alpha_3}\left[\left(\frac{2\sqrt{2\epsilon_f}}{\alpha_2}+1\right)^2 - 1\right]} \tag{2.19}$$

The above equations include the first, second and third phase of the reaction of the sandwich structures at the time of explosion and this equations also gives the deflection, response time, core compression, maximum tensile strain and blast impulse in the sandwich structure. Otherwise, core compression is set at the condensation limit ϵ_D at higher pulses and w is known to scale roughly linearly with $\bar{I}$. At low impulses, the structural reaction time rises linearly with $\bar{I}$, but at high impulses, the structure acts like a strained plastic string, and T is almost independent of the magnitude of $\bar{I}$.

2.1.4 Optimal Geometry Against Air Impulses

The only design parameter for sandwich structure is defined as H/L parameter, where H is core thickness and L is half of plate length. In the case of an optimally designed sandwich structure the core contains about one third of the plate's mass for air blasts. Also, the compression strain ϵ_c, is variated over the considered range but it is generally less than 20%. Moreover, for optimal structures, if the D_{crit}, which is maximum allowed deflection, is equal to 0.25, sandwich structures outperform more efficient than solid plate in an air blast. And again, if $D_{crit} > 0.3$, the profit of sandwich plate over the solid plate is stretching has an advantage on energy distribution. These patterns

match those obtained from a three-dimensional finite element analysis with a limited set of parameters.

CHAPTER 3

3D- FINITE ELEMENT MODEL

In this section, the details of the 3D finite element model and analysis are explained to compare in terms of plastic equivalent strain, von Mises stress and displacement.The core geometry, material model and parameters and boundary conditions used are discussed in detail in this section. For the analysis ABAQUS/ Explicit is used as the finite element software and the results are demonstrate by using its visualization tools..

3.1 Geometry

The geometries required to build the model are selected depending on the initial 1D analysis, and the core geometries were determined accordingly. For the analysis to be made, four core geometries are selected at the beginning, the final core types are determined and a geometry is proposed as final design. These selected geometries are triangular core structure, hourglass core structure, honeycomb core structure and grid core structure.

The selected geometry types are drawn in the SolidWorks CAD program. The length of the drawn pieces is determined as 1840 mm with a width of 600 mm. The heights and sheet thicknesses of the geometries are adjusted according to the equal weight of each geometry per unit surface.

For the triangular core geometry, the height is taken 75.21 mm and the sheet material thickness is 2.92 mm (Fig. 3.1). For the hourglass core geometry, the height is determined as 73.87 mm and the thickness of the sheet material is determined as 1.97 mm. (Fig. 3.2). For honeycomb and grid core geometry, the material height and the sheet

thickness are defined as 70 mm and 1 mm, respectively (Fig.3.3 and Fig. 3.4).

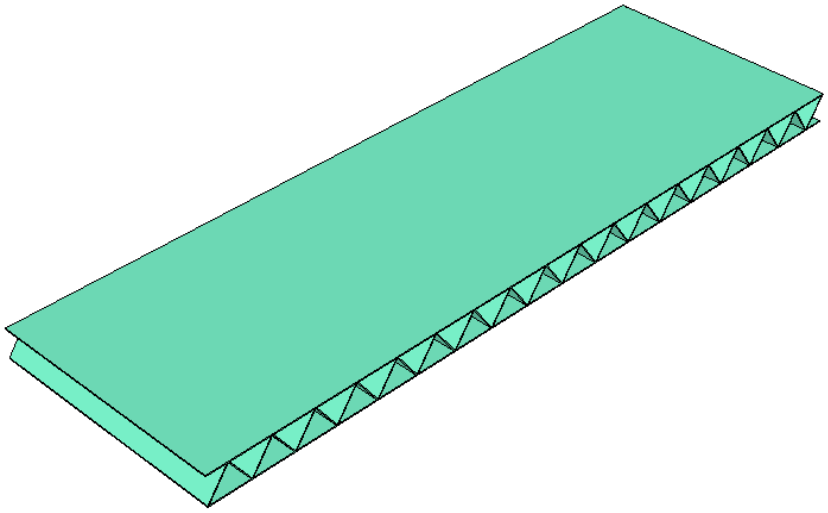

Figure 3.1: Triangular Core Geometry

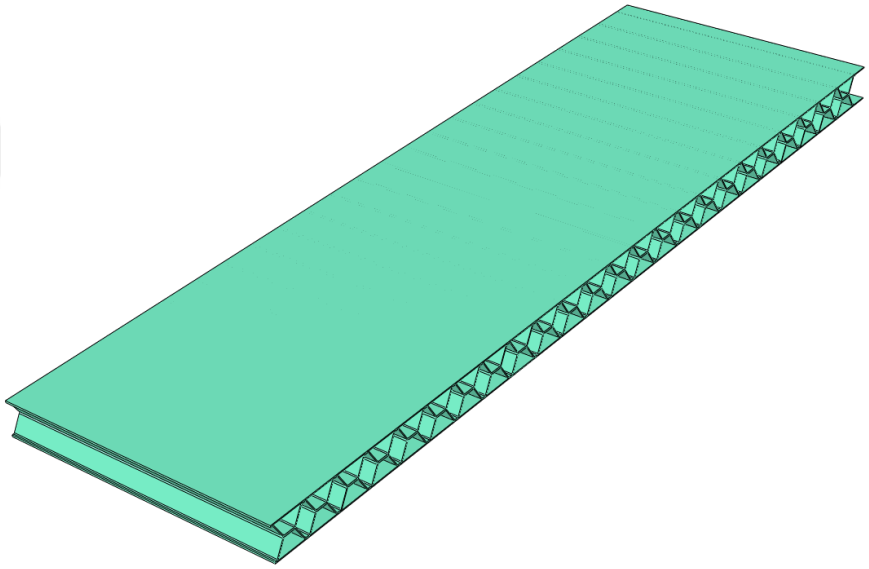

Figure 3.2: Hourglass Core Geometry

The weight per unit surface area of the created geometries are equalized so that an accurate comparison can be provided. An equal volume is obtained by adjusting the thickness of the bottom, top plate and core of the sandwich structures drawn. In this way, the weight per unit surface of the geometries with equal surface area is equalized. These values are shown in the table 4.1.

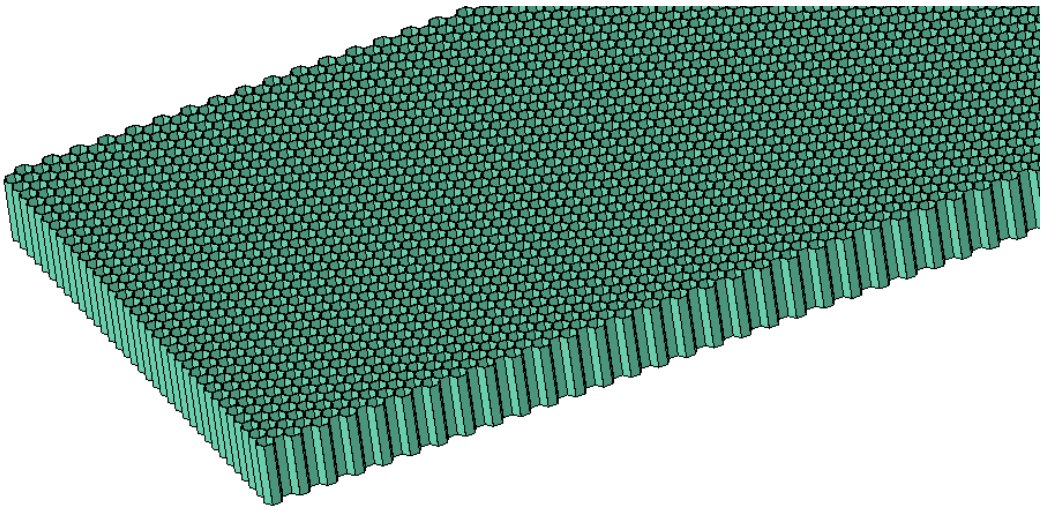

Figure 3.3: Honeycomb Core Geometry

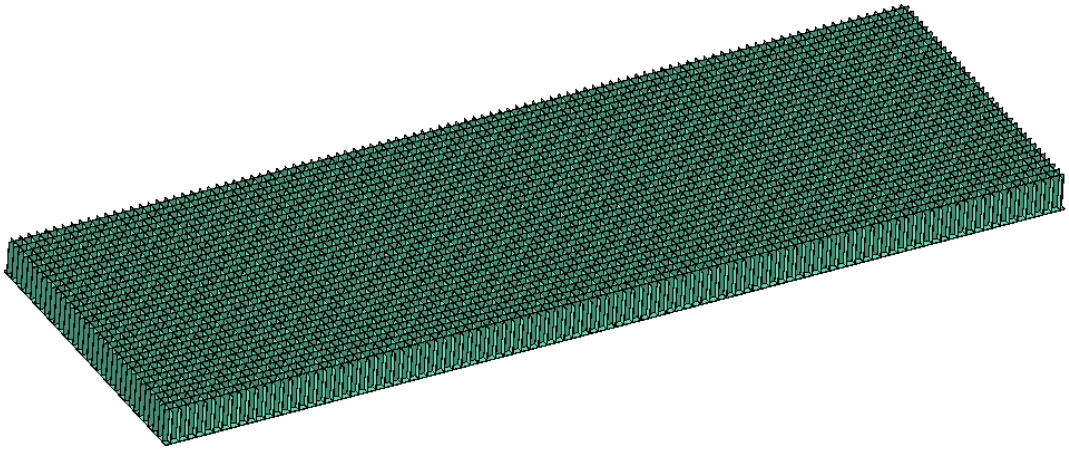

Figure 3.4: Grid Core Geometry

Table 3.1: Mass, Volume and Ratio Table of Created Geometries

Geometry	Volume (m^3)	Surface A.(m^2)	Mass (kg)	Mass/Area(kg/m^2)
Triangular Core	0.010721737	1.104	84	76
Hourglass Core	0.010721869	1.104	84	76
Honeycomb Core	0.010721293	1.104	84	76
Grid Core	0.010721792	1.104	84	76

After the analysis made with 4 different core geometries, 2 candidate geometries are

chosen depending on their performance. These core geometry types, determined on basis of the first analysis results, are created in the test panel dimensions as 405 mm x 405 mm. Again, in these geometries, the weight per unit surface area is equalized and the analysis are performed in the same way. In addition, in the 2 selected geometries, the bottom and top panel sheet thicknesses are taken as 3 mm and the sheet thickness of the core structure is defined as 1 mm. In order to facilitate spot welding of geometries for production.

After the final analysis, the necessary topology optimization is made on the suitable core type and a final geometry is proposed.

After the geometries are created and scaled, after the material model is selected.

3.2 ConWep Blast Model

The gaseous components of explosives detonated in air quickly compress the air and move the air at a speed close to the initial velocity of the explosive. After the explosion, a shock wave with discontinuities in pressure, temperature and velocity occurs with the expansion of the gases released. The shock wave consists of highly compressed air particles that exert pressure on all surfaces they come into contact with as it passes through the air. After the explosion, The pressure at a fixed point in space decays exponentially over time. The time period of an ideal blast wave pressure pulse is normally calculated in fractions of milliseconds. The air blast charge intensity at a point depends on the explosive material used, its mass (m), and the distance between the explosion point and the target point (r). The maximum pressure (P) of an explosive in a free space can be calculated by

$$P = K\left[\frac{m}{r^3}\right] \tag{3.1}$$

and where K is the explosive material constant.

The wave distribution emanating from the source may not always be linear (Fig. 3.5). Moreover, the resulting blast loads for a weak shock are doubled when the shock wave is reflected. But, reflection coefficients of 8 have been recorded for strong shocks

under ideal gas conditions, and up to 20 when real gas effects such as dissociation and ionization of air molecules are taken into account.

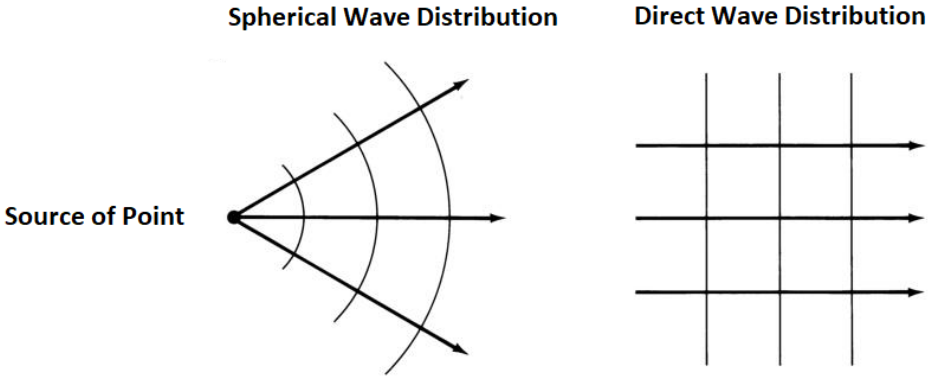

Figure 3.5: Different Wave Distribution Shapes

ConWep (COnventional WEaPons), a blast simulation code developed in 1997 by the US Army Corps of Engineers, was used to estimate the pressure and impulse loads applied to the surface of the test structures examined here [32][33]. The load blast is defined in this case by the ConWep function, which replaces wave propagation with a pressure function. The main feature of the ConWep model is that the pressure is applied to each element separately in a finite element model. Equivalent pressure value created with the developed ConWep model can be written as

$$P(t) = P_{ref} \cos^2 \theta + P_{in}(1 + \cos^2 \theta - 2 \cos \theta) \tag{3.2}$$

where θ is the incidence angle of wave. Also, P_{ref} and P_{in} are pressure value of the reflected pressure wave, the value of the incident pressure wave, respectively.

It can also be said that the ConWep method is based on the application of a relation whose load curve is known to the structure. Using the Friedlander relation, the following equation can be written.

$$P(t) = P_{max}\left[1 - \frac{t - T_a}{T_0}\right] exp\left[\frac{-A\ x\ (t - T_a)}{T_0}\right] \tag{3.3}$$

Where P_{max} is maximum pressure, T_0 and T_a are the time that the pressure is positive

and the time the pressure reaches to the target, respectively. Also, A is the unitless waveform number connected to P_{max}, it represents the coefficient that can take different values for different blasts. These parameters are derived from Kingery and Bulmash calculations [34]. Using the maximum pressure, thrust and time values, the unitless A coefficient is found. Then, using Friedlander equation, blast pressure values in different time periods are derived.

3.3 Johnson-Cook Material Model

In 1983, G. R. Johnson and W. H. Cook developed a material model, which is named Johnson-Cook material model, with their work [35]. The Johnson-Cook model is a multiplier rule. It's a strain-dependent, temperature-dependent viscoplastic model that works well with high strain rates. This model generally uses for under dynamic impact and the materials are affected high strain rates, large strain and high temperature. This model basically constitutes two behaving, which are plasticity and damage.

3.3.1 Johnson-Cook Plasticity Model

Johnson-Cook plasticity is an isotropic hardening model in which the static yield stress is thought to be of the following form.

$$\sigma^0 = \left[A + B(\overline{\epsilon}^{pl})^n\right]\left(1 - \hat{\theta}^m\right) \tag{3.4}$$

where σ^0 is flow stress, ϵ^{pl} is plastic strain, and c is a thermal softening coefficient. Moreover, A,B and n is a define material parameter and yield stress of material, hardening modulus and hardening exponent, respectively. Also θ^m is defined as a non-dimensional temperature and is determined as

$$\hat{\theta} = \begin{cases} 0, & \text{for } \theta < \theta_{transition} \\ (\theta - \theta_{transition})/(\theta_{melt} - \theta_{transition}), & \text{for } \theta_{transition} \leq \theta \leq \theta_{melt} \\ 1, & \text{for } \theta > \theta_{melt} \end{cases}$$

where θ is the room temperature, θ_{melt} is melting temperature and $\theta_{transition}$ is the transition temperature defined as the temperature at or below which the yield stress is unaffected by temperature.

When $\theta \geq \theta_{melt}$, the material will not behave like a solid, and there will not be shear resistance because σ^0=0. For most materials, the $(\theta - \theta_{transition})/(\theta_{melt} - \theta_{transition})$, condition is generally used for blast analysis.

For Johnson-Cook material model, strain rate dependence assumes that

$$\overline{\sigma} = \sigma^0(\overline{\epsilon}^{pl}, \theta)R\left(\dot{\overline{\epsilon}}^{pl}\right) \tag{3.5}$$

and

$$\dot{\overline{\epsilon}}^{pl} = \dot{\epsilon}_0 \; exp\left[\frac{1}{C}(R-1)\right] \quad \text{for} \quad \overline{\sigma} \geq \sigma^0, \tag{3.6}$$

Where $\overline{\epsilon}$ is the yield stress at non-zero strain rate and $\dot{\epsilon}_0$, C are the material parameters measured below the transition temperature. So, the yield stress is expressed include rate dependency as

$$\sigma^0 = \left[A + B(\overline{\epsilon}^{pl})^n\right]\left[1 + C \; ln\left(\frac{\dot{\overline{\epsilon}}^{pl}}{\dot{\epsilon}_0}\right)\right]\left(1 - \hat{\theta}^m\right) \tag{3.7}$$

In this equation 3.7, the values A, B, n, m, $\theta_{transition}$, θ_{melt} and for rate dependence, C and $\dot{\epsilon}_0$ should be defined in the material model [35].

3.3.2 Johnson-Cook Damage Model

A dynamic failure model is provided by the Johnson-Cook material model, which is only suitable for metals with a high strain rate of deformation. The Johnson-Cook dynamic damage model is based on the equivalent plastic strain at integration points of elements and damage is assumed when the damage parameter surpasses 1. This damage parameter, ω, can be written as

$$\omega = \sum \left(\frac{\triangle \overline{\epsilon}^{pl}}{\overline{\epsilon}_f^{pl}} \right) \tag{3.8}$$

where$\triangle \overline{\epsilon}^{pl}$ is amount of increase of the equivalent plastic strain and $\overline{\epsilon}_f^{pl}$ is the strain at failure [**?**]. The summation of the equation is applied to all of the analysis' increments. $\overline{\epsilon}_f^{pl}$ is thought to be based on the rate of non-dimensional plastic strain rate, $\dot{\overline{\epsilon}}^{pl}/\dot{\epsilon}_0$, and a dimensionless pressure-deviatoric stress ratio p/q where p is the stress of pressure and q is the von Mises stress. Also, non-dimensional temperature, $\hat{\theta}$ is defined in the Johnson-Cook damage model. So, the general equation can be combined as

$$\overline{\epsilon}_f^{pl} = \left[d_1 + d_2 exp\left(d_3 \frac{p}{q} \right) \right] \left[1 + d_4 ln\left(\frac{\dot{\overline{\epsilon}}^{pl}}{\dot{\epsilon}_0} \right) \right] (1 + d_5 \hat{\theta}) \tag{3.9}$$

where d_1, d_2, d_3, d_4, d_5 is material failure parameters and when defining the equation, of Johnson-Cook damage model, it is necessary to ensure these values.

The application of the Johnson-Cook dynamic damage model requires the use of Johnson-Cook plasticity, but generally does not require the Johnson-Cook strain rate dependency. Only if the Johnson-Cook strain rate dependency is established, the rate-dependent term in the Johnson-Cook dynamic damage criterion is included.

Initially, only a single material is assign to the complete geometry for the numerical analysis . High strength armour steel, which are widely used in the defence industry, is selected as the material. QP1180 ultra-high strength steel,is used as the reference material. Also, Johnson-Cook material model is adopted as the material model. The material parameters for QP1180 are provided by FNSS Defence System. The material densities are taken as 7.85×10^{-9} $tonne/mm^3$. Also, the young modulus and poisson's ratio is 210000 MPa and 0.3, respectively. Johnson-Cook plasticity parameters of this material are provided in Table 3.2.

Table 3.2: QP1180 High Strength Steel Johnson-Cook Material Plasticity Parameters

A (Mpa)	B (MPa)	n	m	C	$\dot{\epsilon}(s^{-1})$
977.5	1191	0.5141	0	0.003	0.001

As mentioned before, after the analysis made with the initial geometries, two geometries are selected. According to materials supplied from FNSS defence industry, S700MC steel is used for 3 mm sheet plate and TRIP1180 steel for 1 mm steel. Johnson-Cook plasticity parameters of these selected materials are presented for S700MC steel in Table 3.3 and TRIP1180 steel in Table 3.4.

Table 3.3: S700MC High Strength Steel Johnson-Cook Material Plasticity Parameters

A (MPa)	B (MPa)	n	m	T_m	T_r	C	$\dot{\epsilon}(s^{-1})$
730.24	2464.49	1.1244	1.2895	1200	20	0.003	0.001

Table 3.4: TRIP1180 High Strength Steel Johnson-Cook Material Plasticity Parameters

A (Mpa)	B (MPa)	n	m	T_m	T_r	C	$\dot{\epsilon}(s^{-1})$
761.94	112.89	0.2597	2.109	1200	20	0.003	0.001

3.4 Load and Interaction

In this section, determination of bursting force load and distance, defining boundary conditions and other settings related to the boundary conditions of the analysis will be presented.

In this study, all the finite element analysis are dynamic explicit analyses. Very small time increments are used in this method for the efficient and an explicit central-difference time integration rule is adopted. The step time period is 0.003 seconds.

In the blast simulation using the ConWep method described in the previous sections, 1 kg TNT is determined as the explosion mass for the first geometries used. Then, ConWep analyses are carried out using 1 and 3 kg TNT for the two selected geometries and a final core geometry is proposed.

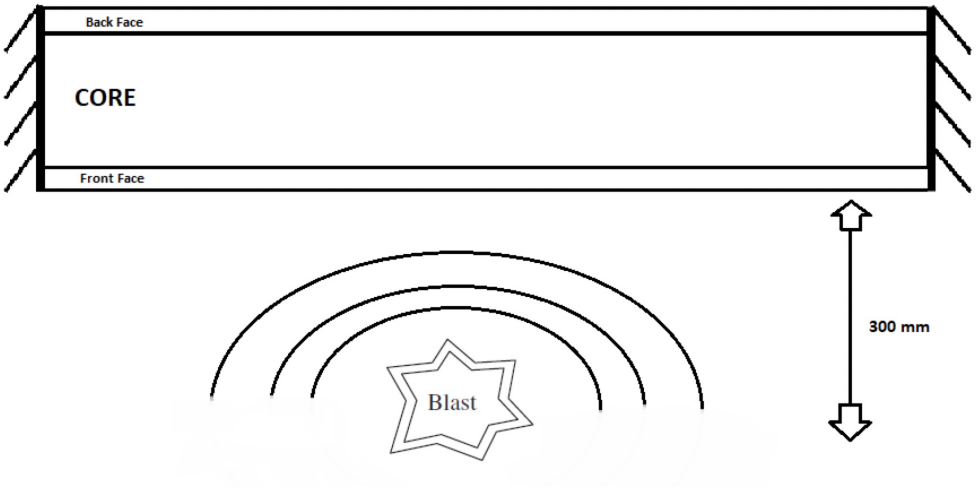

Figure 3.6: Explosion Schematic Example and Boundary Conditions Used in Reference Geometries

In the analysis, the stand of distance is taken as 300 mm to the sandwich structure as shown in the figure (Figure 3.6) in all geometries and simulations. This distance has been determined according to the standards. The reference point set 300 mm away from the front surface of the sandwich structure is defined by the ConWep method ABAQUS / Explicit. The system is analysed by calculating the effects of the blast on the reference point on the structure. In addition, detonation time is set as 0.0001 seconds for all analyses performed in this study.

In the definition of the boundary conditions, the short edges are kept as fixed as shown in the figure (Figure 3.7). This definition of boundary conditions is made only for the lower and upper panels and the core geometry is left free to observe the motion at the moment of explosion.

For analysis made with two selected geometries and the geometry to be proposed, the boundary condition on the four edges of the lower and upper panel is defined as fixed/encastre thus the effect of displacement and rotation in 3 axes is zero. Again in this condition, no boundary condition is defined for the core geometry.

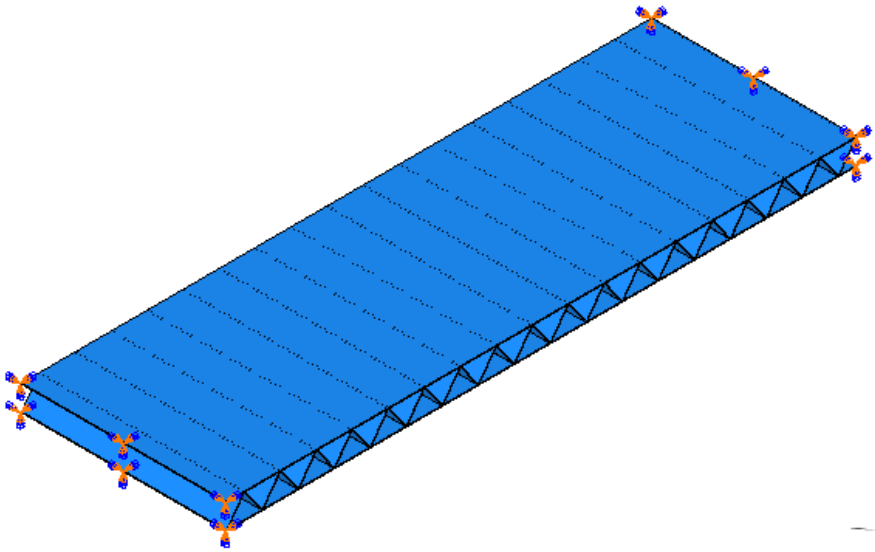

Figure 3.7: Example of Boundry Conditions Used in Reference Geometries

In addition, all the analysis are performed with the parallelization option of the ABAQUS solver by utilizing 40 cores for each analysis.

3.5 Mesh

This section presents the mesh structure in the created finite element model. Explicit element library is used when meshing all geometries and also linear elements are selected as the geometric order.

In all analyses, mesh is made by using hexagonal elements. However, in elements with complex geometries, a triangular element type is used to mesh more easily. The element types used are named as C3D8R and C3D4 in the ABAQUS software. Also reduced integration is used. The locking phenomena reported in the C3D8 element are not visible due to the reduced integration. The C3D8R element's integration point is positioned in the centre of the element, since it is a reduced type. To capture a stress concentration at a structure's boundary, smaller elements are required.

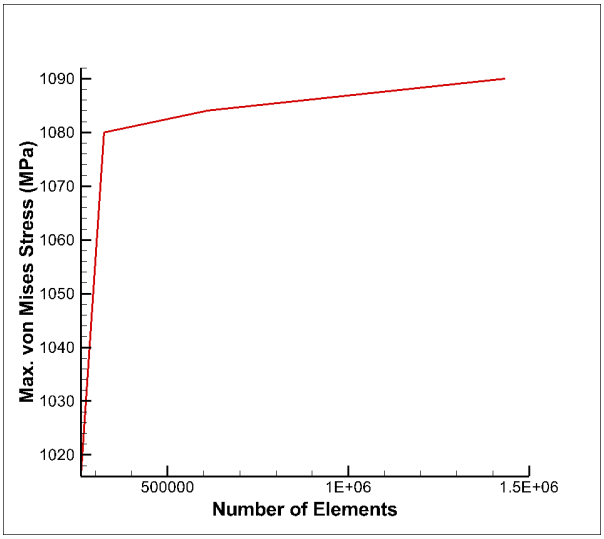

Figure 3.8: Total Element Number vs Max. Stress at the End Of Analysis Graph

Table 3.5: Total Element Number and Computational Time Comparison

Element Lenght (mm)	Total Element Number	Computational Time (s)
5.5	260074	762
5	323640	879
3.5	612009	2300
2	1435800	2760

Before meshing the geometries, mesh sensitivity analysis is performed for a single geometry. Geometries are meshed with different mesh resolutions. Then, the total number of elements - the maximum stress at final time plot is evaluated (Figure 3.8). With this graph drawn, the actual time elapsed during the analysis is calculated (Table 3.5), and the optimal element size to be applied is found when meshing.

Considering the analysis results, there is a difference between the 5.5 mm and 5 mm element lengths according to the calculated stress values. However, below 5 mm element length, the stress value converges into a acceptable range. Also, when the total time is taken into account, there is approximately 2.5 times the difference according to the closest value and 3 times the difference according to the fine mesh. Considering this time difference, 5 mm was chosen as the ideal element size and adopted to all geometries.

The total number of elements formed after mesh parameters is shown in Table 3.6. The total number of elements in some geometries, such as honeycomb core geometry, is quite high due to the dense core structure Parallel to this, the analysis time has also been prolonged.

Table 3.6: Total Element Number of All Reference Geometries

Core Geometry	Total Element Number
Triangular Core Geometry	173040
Hourglass Core Geometry	323640
Honeycomb Core Geometry	2783106
Grid Core Geometry	324093

Mesh details of triangular core geometries (Fig. 3.9), hourglass core geometries (Fig. 3.10), honeycomb core geometries (Fig. 3.11) and grid core geometries (Fig. 3.12) are shown below.

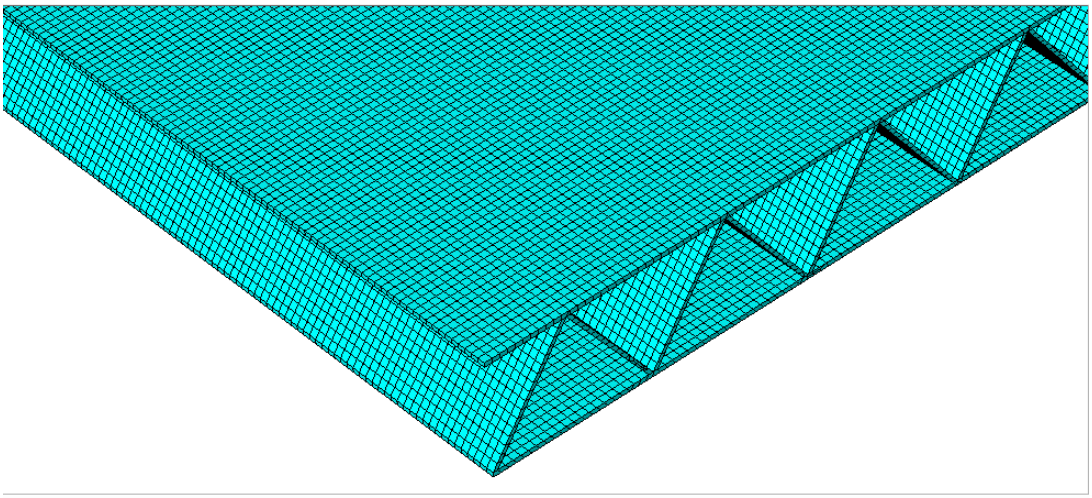

Figure 3.9: Mesh Detail of Triangular Core Geometry

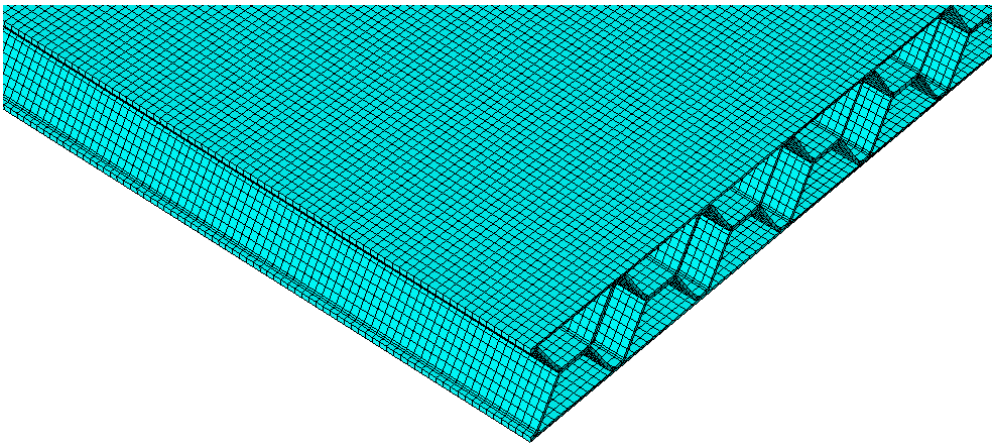

Figure 3.10: Mesh Detail of Hourglass Core Geometry

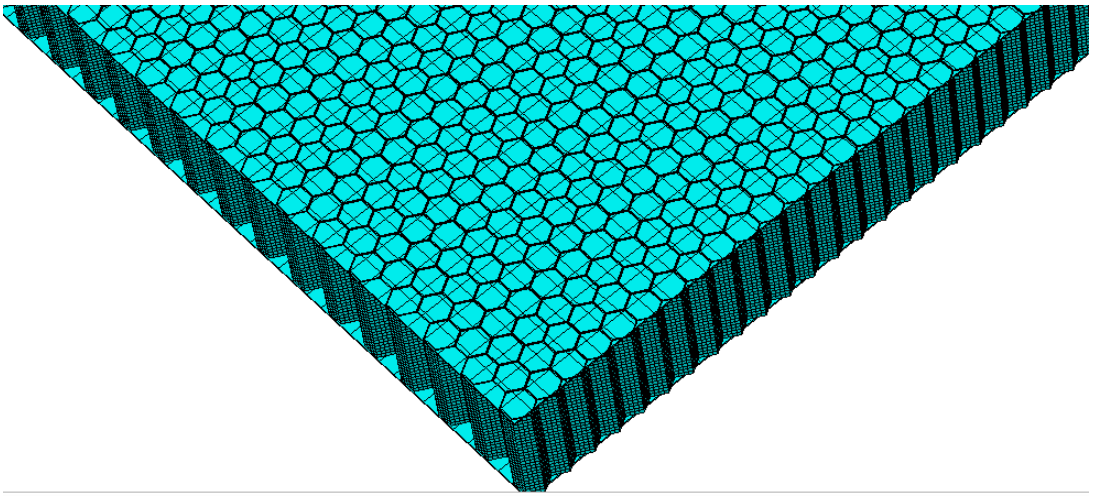

Figure 3.11: Mesh Detail of Honeycomb Core Geometry

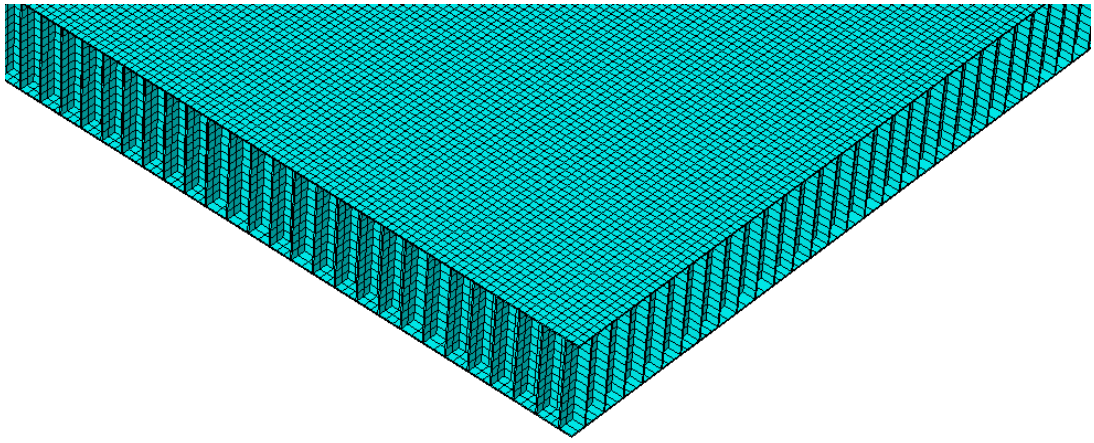

Figure 3.12: Mesh Detail of Grid Core Geometry

After the mesh created in the ABAQUS/Explicit software, the geometries were analysed. Afterwards, the results of the geometries were examined in the visualization tool of ABAQUS and comparisons with the desired parameters are made in the next section.

CHAPTER 4

NUMERICAL RESULTS OF FINITE ELEMENT SIMULATIONS

The previous section was about comprehensive explanations of generating geometry, ConWep method, material models and mesh standards. In this section, we present the numerical simulations to show the analysis of the generated 3-D models. Also, necessary optimizations are made and a new core geometry is proposed according to the numerical results.

9 node points selected from the region where the deformations are most intense are taken as a 3×3 system and the evaluations are made by taking the average of the values shown by these nodal points. The results obtained after the analysis of the geometries created by equalizing the amount of mass per unit surface area and the analysis with constant material parameters gave us the opportunity to compare the Von Mises stress, equivalent plastic strain and deformation.

First of all, the results obtained by comparing the equivalent plastic strain, Von Mises stress and displacement results of the models created with equal reference values gives an idea about the energy absorption and deformation properties of the reference geometries against blast loads. Then, according to these values, analyses will be continued over two core geometries.

The deformation maps of the models used as the reference core geometry, as well as the plastic equivalent strain, von Mises stress and displacement results from the node set regions are shown below (Fig. 4.1, Fig. 4.2, Fig. 4.3, Fig. 4.4).

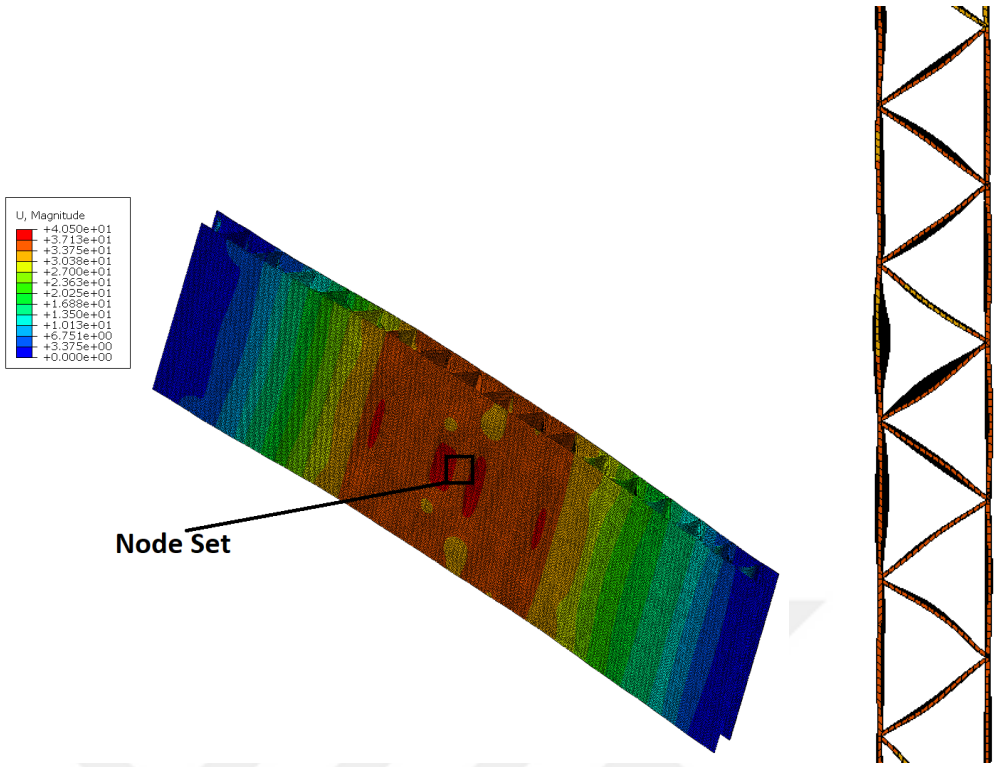

Figure 4.1: Deformed State of Triangular Core Geometry and Selected Node Set Region

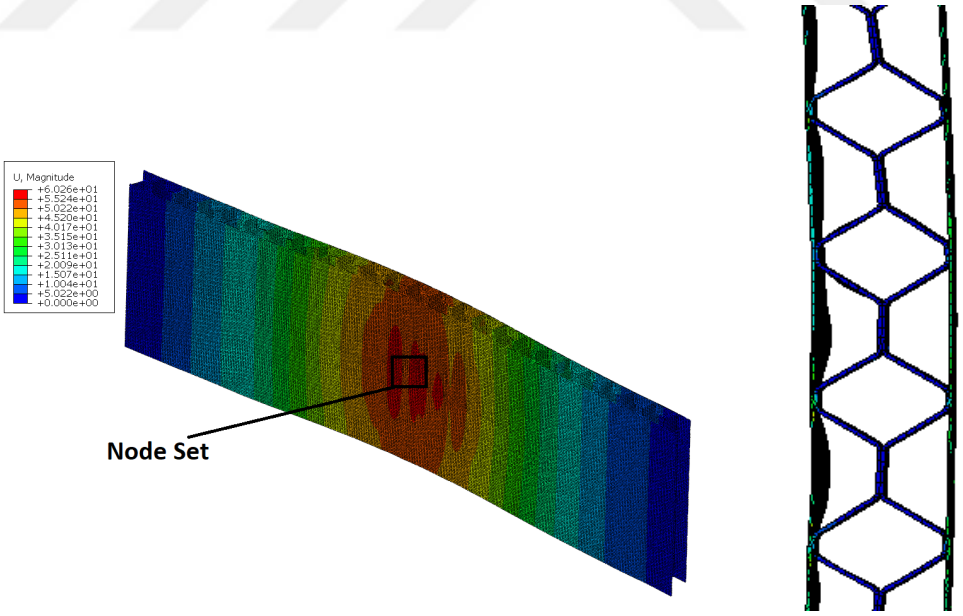

Figure 4.2: Deformed State of Hourglass Core Geometry and Selected Node Set Region

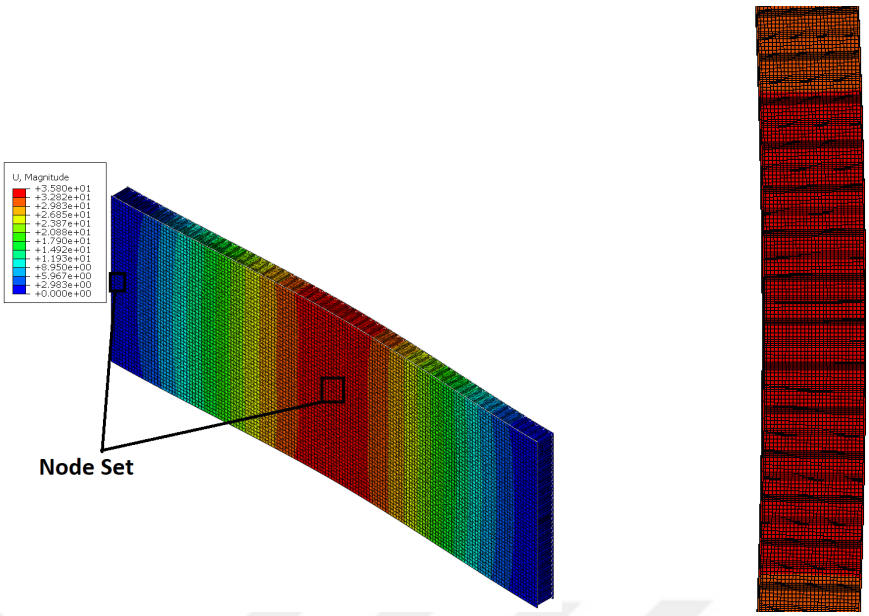

Figure 4.3: Deformed State of Honeycomb Core Geometry and Selected Node Set Region

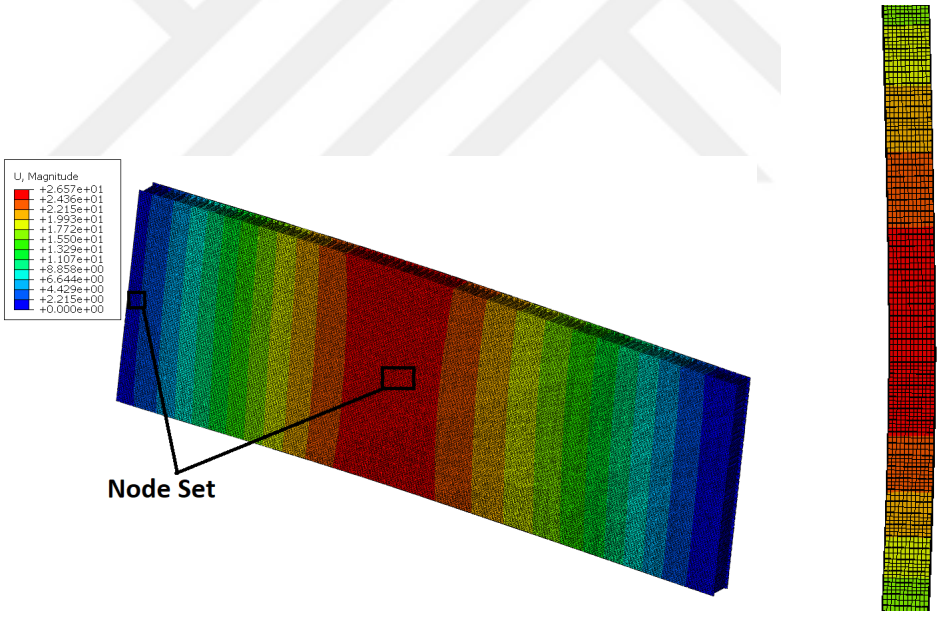

Figure 4.4: Deformed State of Grid Core Geometry and Selected Node Set Region

By averaging the values taken from the selected nodal regions, the values are calculated and the four core geometries are compared with each other in this way. The plots created with these values are shown in Fig. 4.5, Fig. 4.6 and Fig. 4.7.

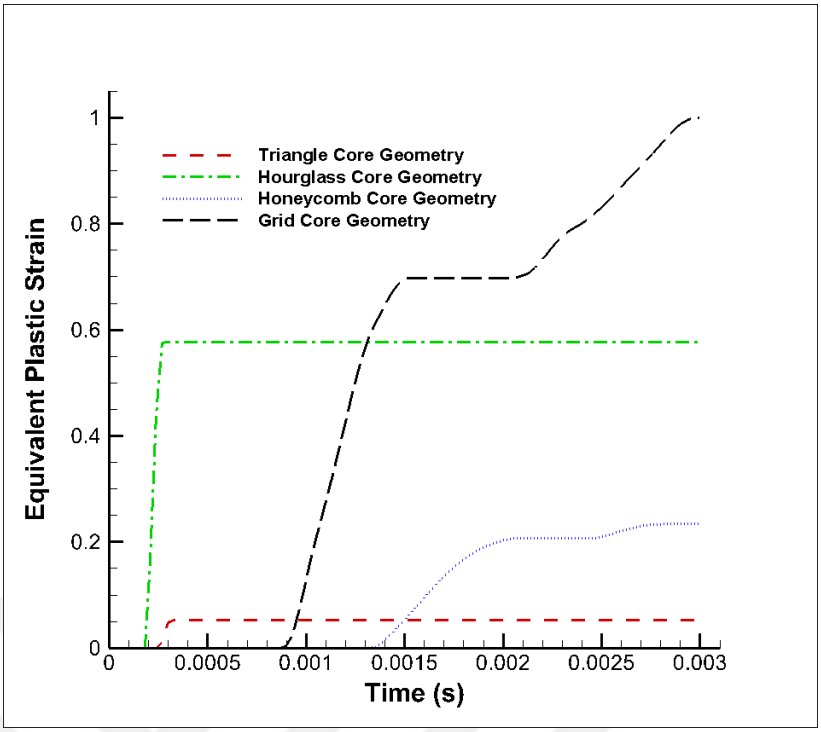

Figure 4.5: Graph of Normalized Equivalent Plastic Strain Comparison of 4 Different Models Created

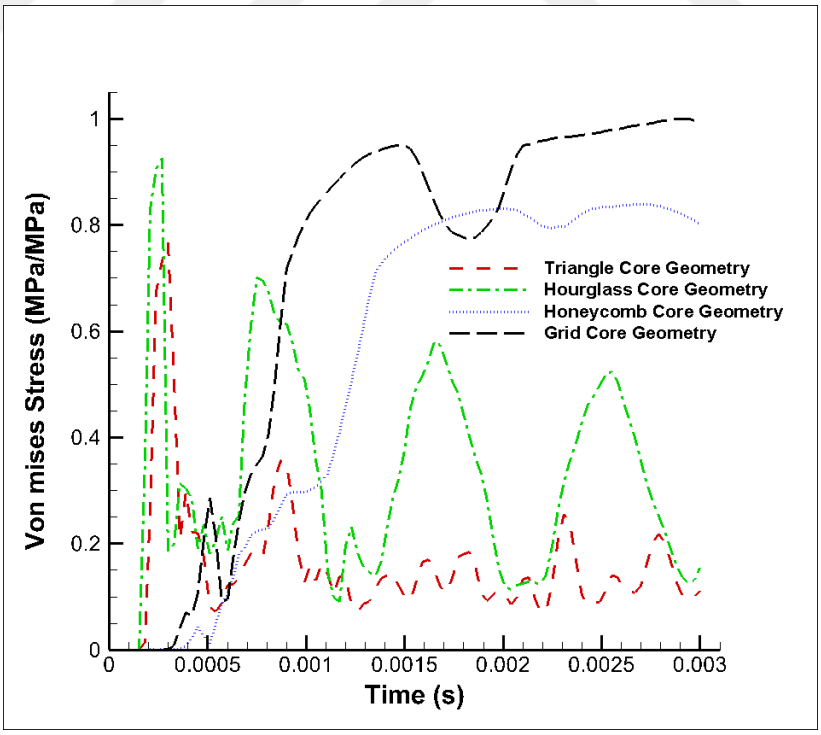

Figure 4.6: Graph of Normalized von Mises Stress Comparison of 4 Different Models Created

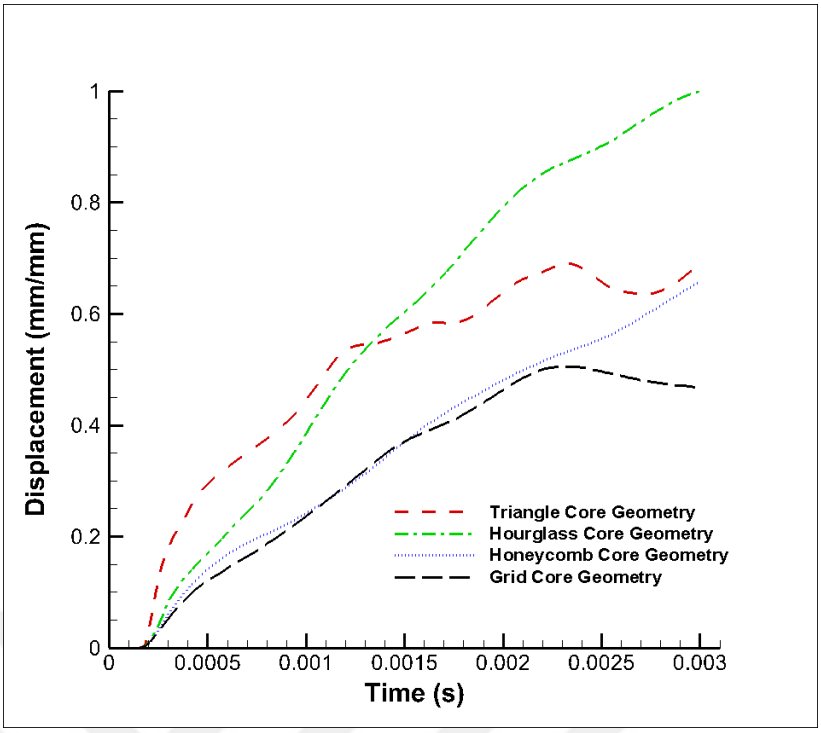

Figure 4.7: Graph of Normalized Displacement Comparison of 4 Different Models Created

The first observation we have made for results of the analysis is that the triangular core, hourglass core, the honeycomb and the grid core structures exhibit two different characteristics. The energy absorption capacity of the triangular core and hourglass core structures, which is topologically more prone to buckling, is higher than the honeycomb and the grid structures, but due to the magnitude of the deformation that occurred during explosion, the values of the relative displacements are measured higher.

In addition, when the current fixed boundary conditions and strain values are compared, the honeycomb and the grid core geometries are observed quite stiff the von Mises stress distributions scatter from the focal point to the edges and the maximum strain value occurs in the region where the boundary conditions are defined, not at the maximum displacement point. As shown in the Figure 4.3 and 4.4 while this situation does not create a problem when comparing the performance of the geometries within itself, it will not provide realistic data in terms of predicting the general protective performance of the mine kit to be designed.

In accordance with the previous analysis, honeycomb and grid core structures, which are mechanically more resistant to buckling and bending, have lower energy absorption capacity than other geometries, besides the deformation remains mostly in the elastic regime and the displacement values are low. When these two different geometries are compared among themselves, hourglass core and grid core, which is cheaper and easier to manufacture compared to the honeycomb core, are selected as candidate geometries and it is concluded that they should form the basis for further analysis to be carried out.

Selected core geometries are plotted in mine test kit dimensions, as previously mentioned, measuring 405 mm x 405 mm. In addition, in order to equalize the areal density, the spacing of the grid geometry are increased and the height of both geometries has been adjusted to 74 mm. For the convenience of manufacturing the thickness of the upper and lower panels taken as 3 mm and the sheet thickness of the core geometry is 1 mm. Because the ratio used in spot welding is generally three to one. Hourglass core geometry and grid core geometry are shown in Figure 4.8 and Figure 4.9.

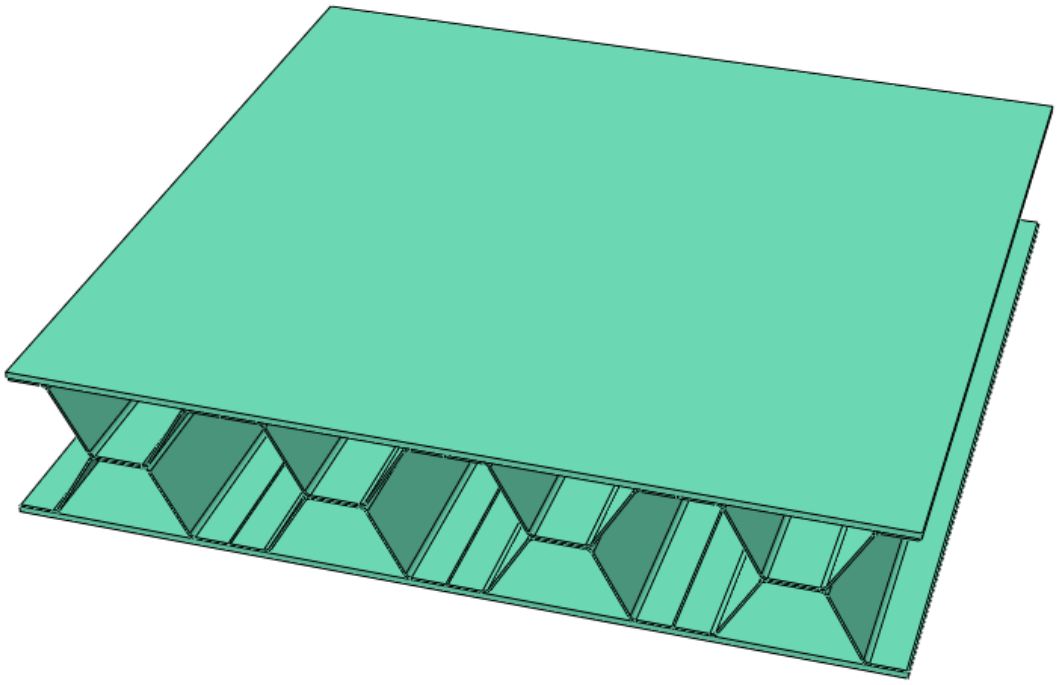

Figure 4.8: Modified Hourglass Core Geometry

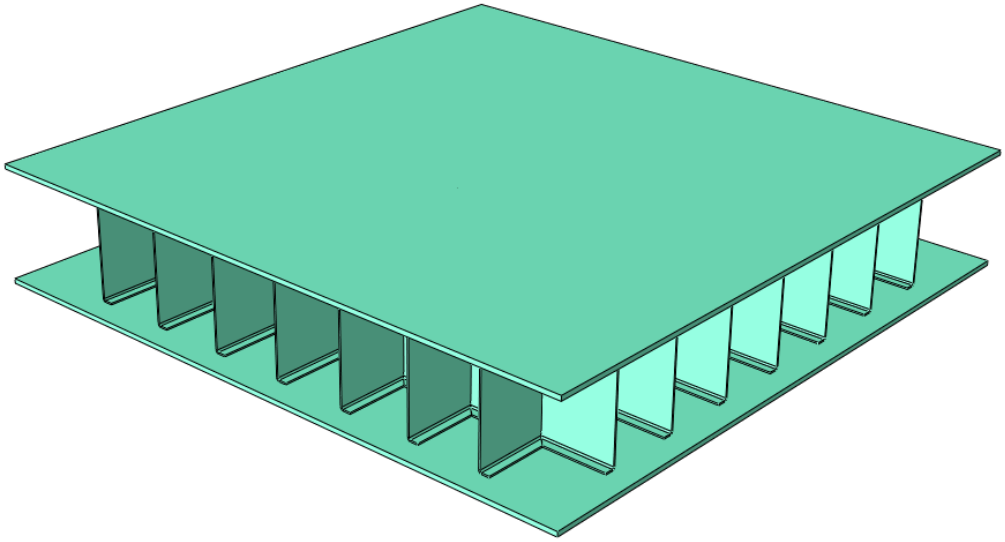

Figure 4.9: Modified Grid Core Geometry

The mass/area ratios of the created geometries are again equalized (Table 4.1) and analyses are performed for the same boundary conditions. In addition, the material used is assigned as S700MC for the lower and upper panels, TRIP1180 for the core geometry, as it is stated in the previous sections, and the Johnson-Cook material model is selected for the material response.

Table 4.1: Mass, Volume and Ratio Table of Created Geometries

Geometry	**Volume** (m^3)	**Surface A.**(m^2)	**Mass** (kg)	**Mass/Surface A.**(kg/m^2)
Hourglass Core	0.0142698	0.164025	11.2	68.29
Grid Core	0.0138697	0.164025	10.9	66.45

In addition, the TNT mass used for the explosion in these analyses is set as 1 kg and 3 kg.The stand of distance is also set to 300 mm. The mesh structure used is determined to be the same as the reference analyses.

After the analysis, the average of the 9 nodal values taken from the 3x3 system determined from the selected regions is taken and the von Mises stress, equivalent plastic strain and displacement values of the geometries are compared. In addition, von Mises

stress and equivalent plastic strain values in the core are found for the hourglass core geometry. The total analysis time and detonation time are not changed, and they are kept constant as 0.003 seconds and 0.0001 seconds used in the reference analyses.

For hourglass geometry deformation maps with 1 kg TNT and selected node set regions after the analysis are shown in Figure 4.10 and with 3 kg TNT and selected node set region are shown in Figure 4.11. Figure 4.12 shows the deformation images formed by 1 kg TNT explosion and the selected node set region, and Figure 4.13 shows the deformed state maps and node set region formed by 3 kg TNT explosion for grid geometry. In addition, the node set region selected from the core structure in hourglass geometry and the node set region selected from the core structure in grid geometry are shown in Figure 4.14.

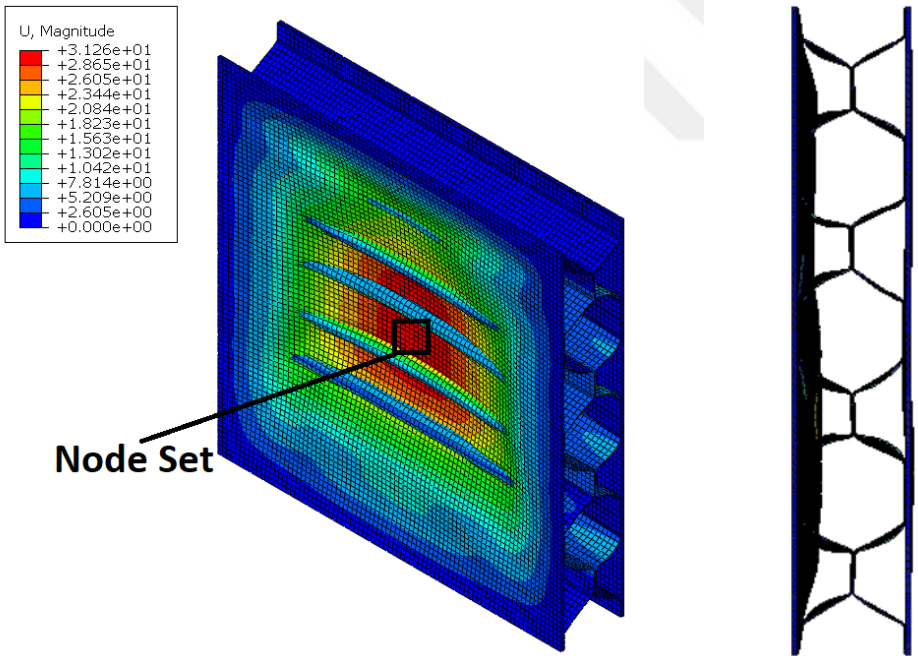

Figure 4.10: Deformed State of Hourglass Core Geometry with 1 kg TNT and Selected Node Set Region

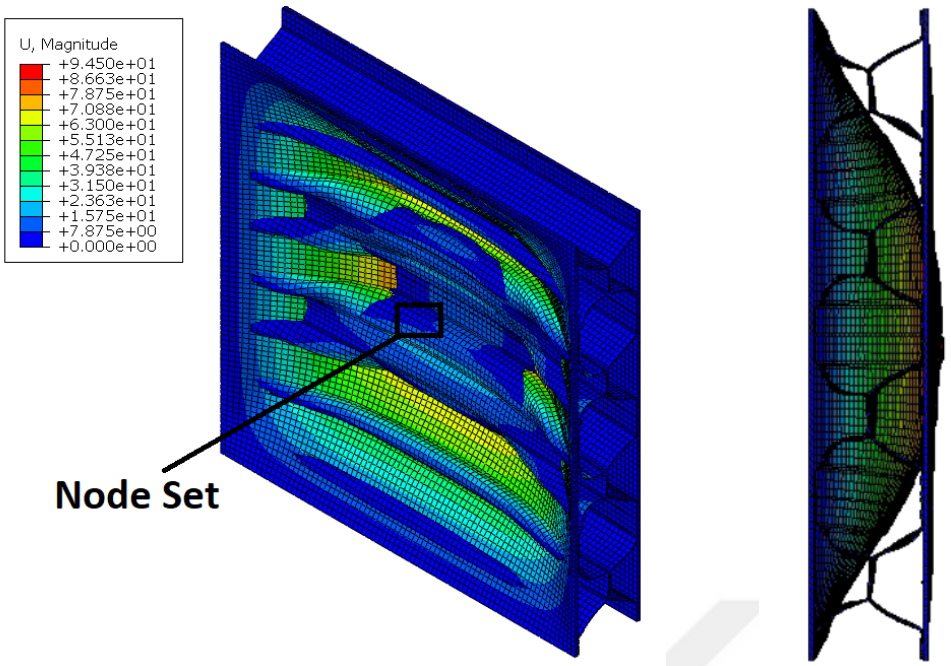

Figure 4.11: Deformed State of Hourglass Core Geometry with 3 kg TNT and Selected Node Set Region

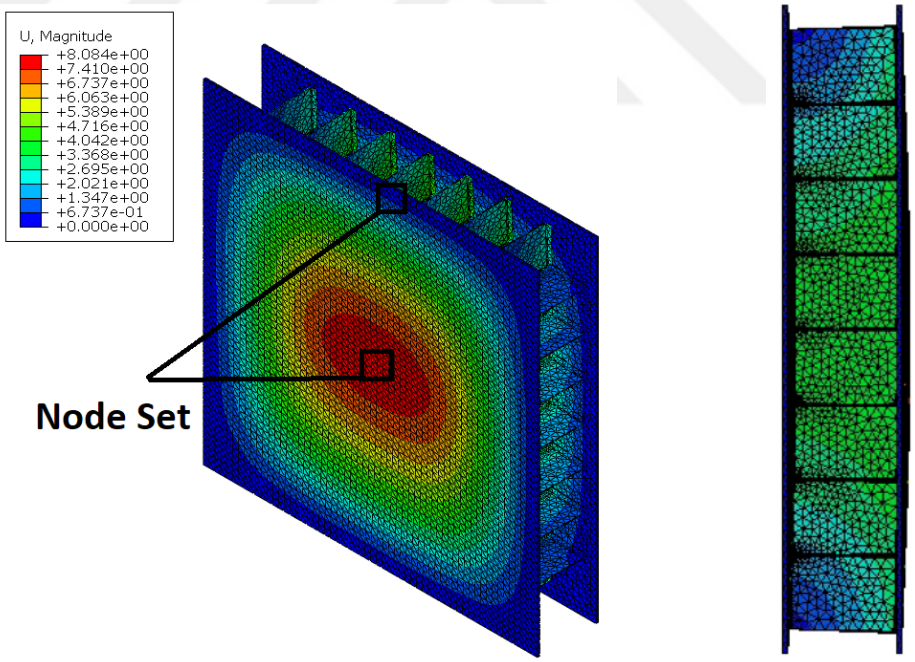

Figure 4.12: Deformed State of Grid Core Geometry with 1 kg TNT and Selected Node Set Region

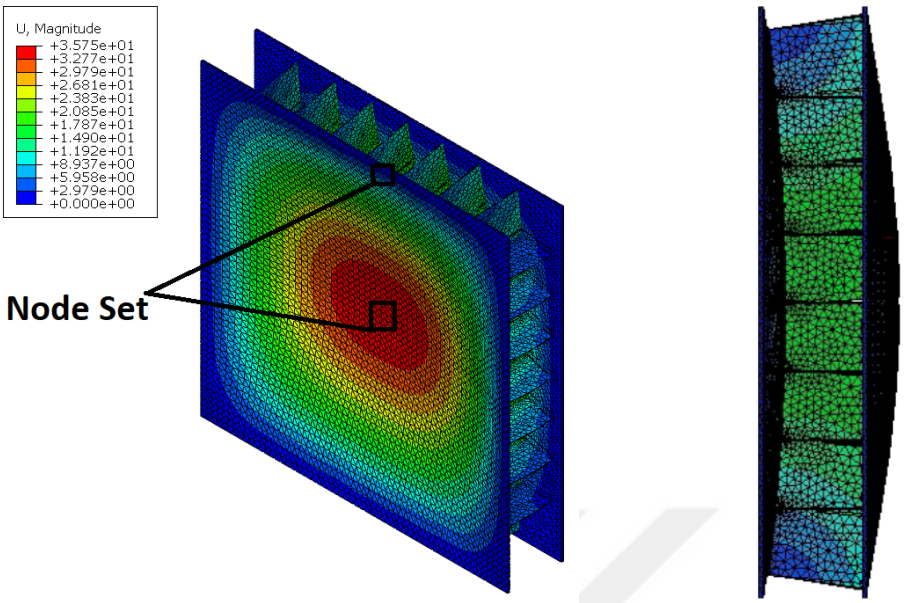

Figure 4.13: Deformed State of Grid Core Geometry with 3 kg TNT and Selected Node Set Region

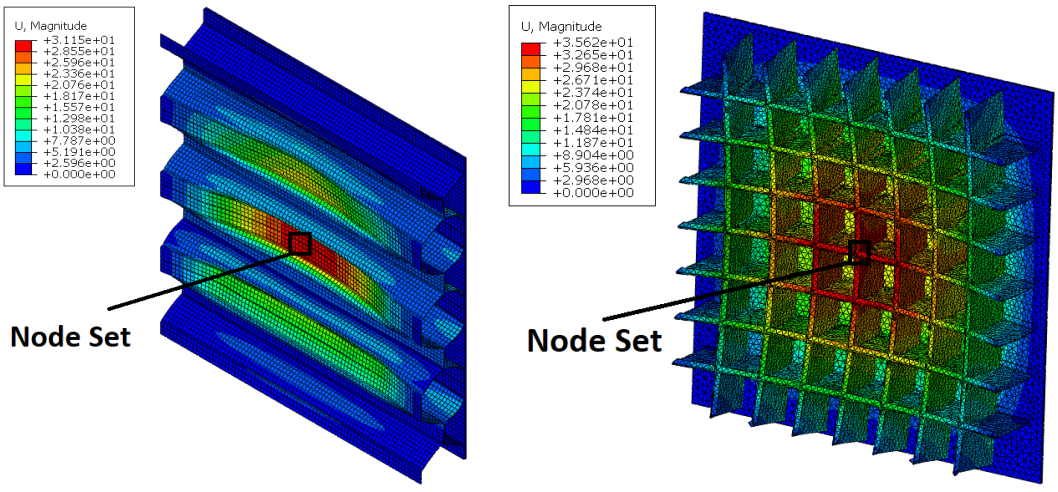

(a) Hourglass Core Geometry (b) Grid Core Geometry

Figure 4.14: Node Set Region from Core Structure

The plots created by averaging the values taken from the regions shown in the figures allow us to compare the core geometries among each other. The graphs of von Mises stress, plastic equivalent strain and displacement for the blast load 1 kg and 3 kg TNT and for reference material (QP1180) and materials to be used in production (S700MC, TRIP1180) separately.

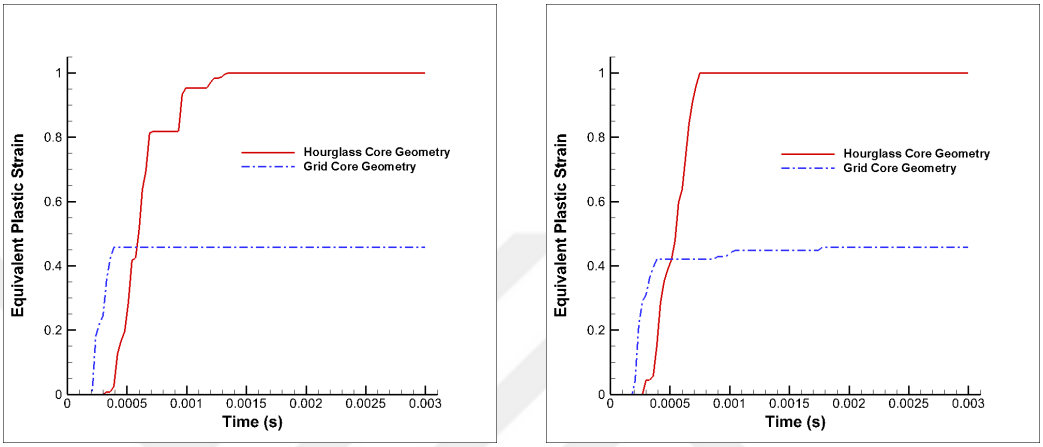

(a) With QP1180 (b) With S700MC and TRIP1180

Figure 4.15: Normalized Equivalent Plastic Strain Comparison Graph of 1 Kg TNT explosion

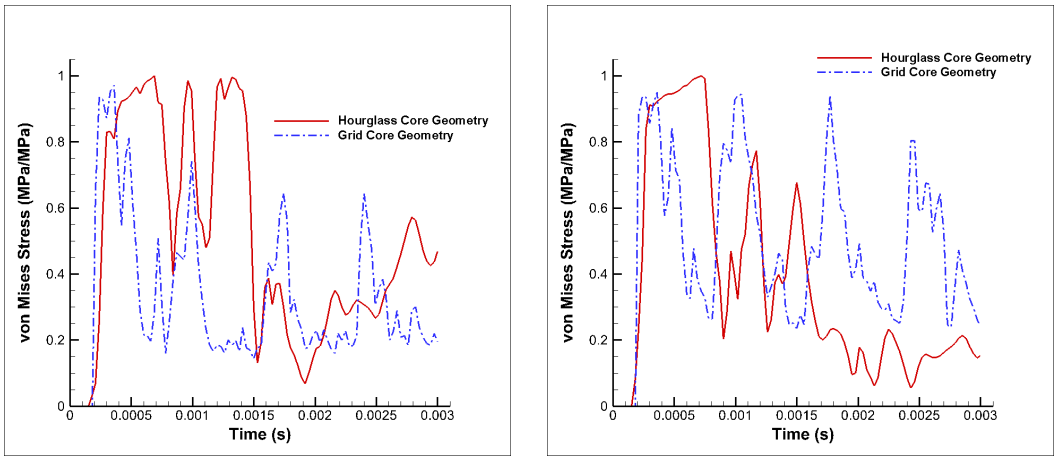

(a) With QP1180 (b) With S700MC and TRIP1180

Figure 4.16: Normalized von Mises Stress Comparison Graph of 1 Kg TNT explosion

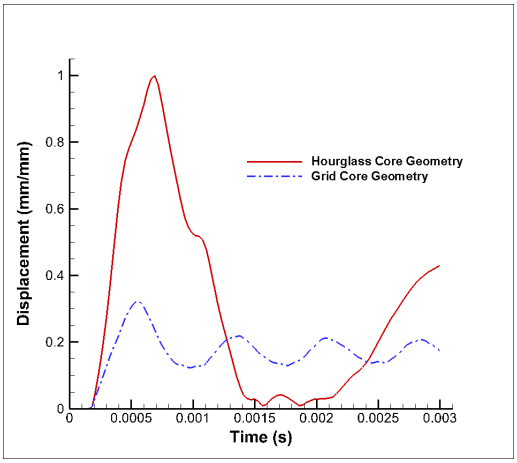

(a) With QP1180

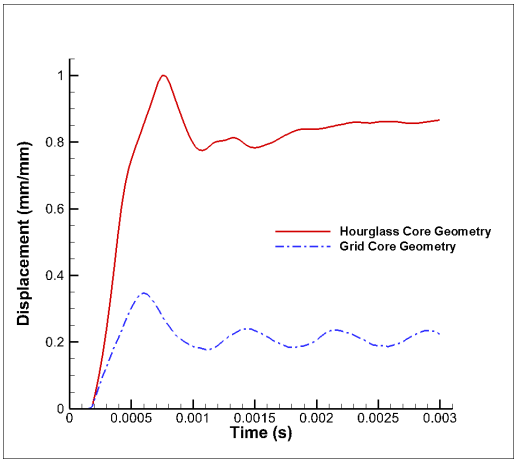

(b) With S700MC and TRIP1180

Figure 4.17: Normalized Displacement Comparison Graph of 1 Kg TNT explosion

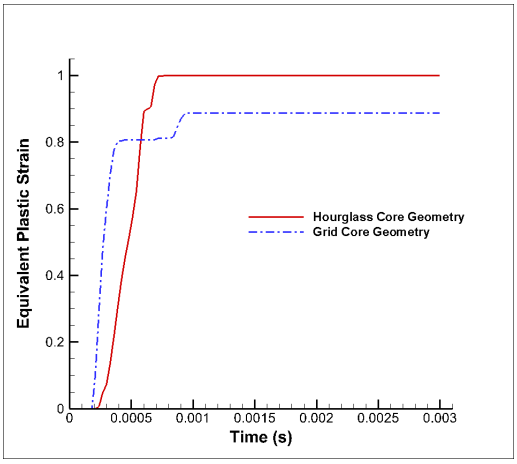

(a) With QP1180

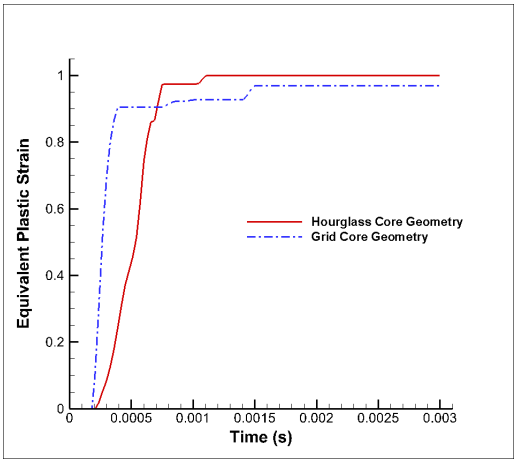

(b) With S700MC and TRIP1180

Figure 4.18: Normalized Equivalent Plastic Strain Comparison Graph of 3 Kg TNT explosion

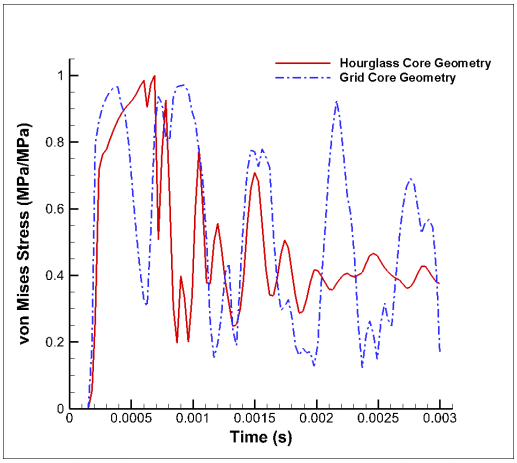

(a) With QP1180

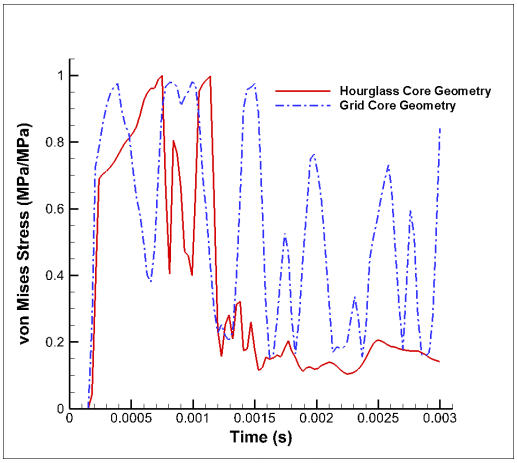

(b) With S700MC and TRIP1180

Figure 4.19: Normalized von Mises Stress Comparison Graph of 3 Kg TNT explosion

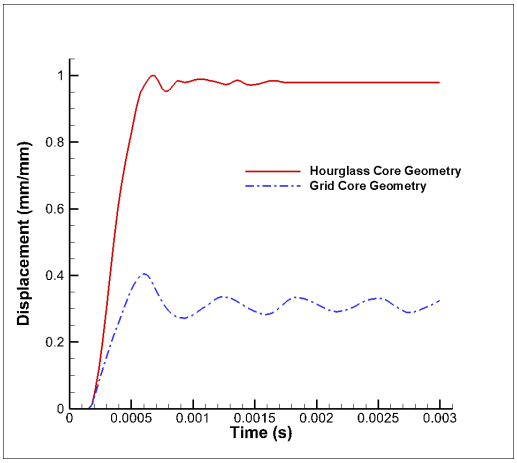

(a) With QP1180

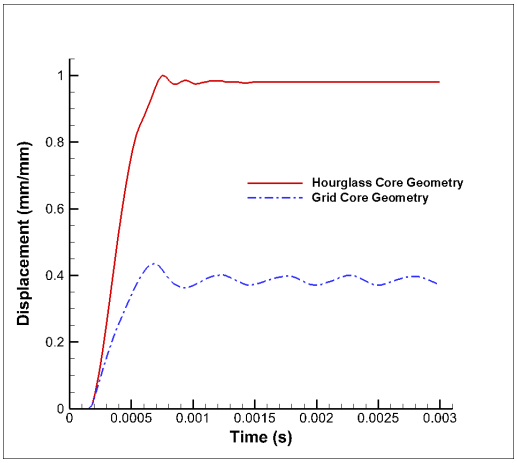

(b) With S700MC and TRIP1180

Figure 4.20: Normalized Displacement Comparison Graph of 3 Kg TNT explosion

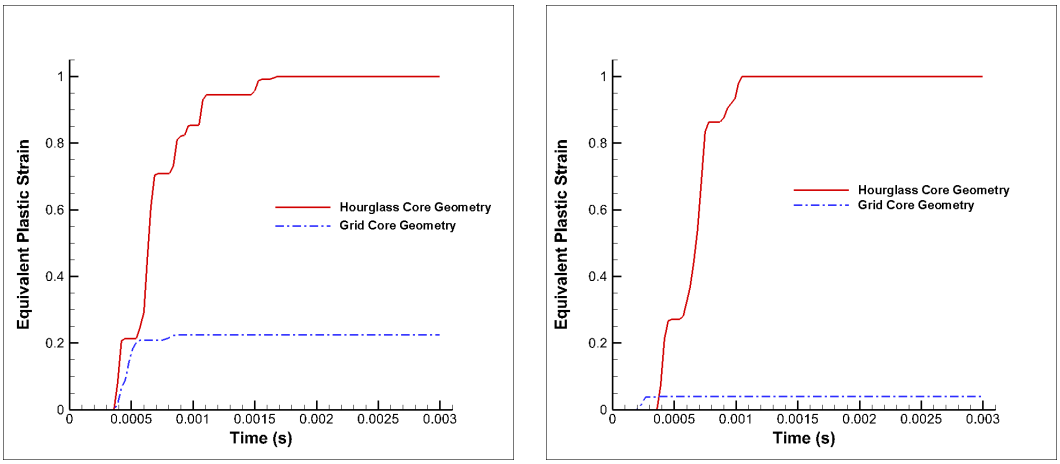

(a) With QP1180 (b) With S700MC and TRIP1180

Figure 4.21: Normalized Equivalent Plastic Strain Comparison Graph in Core Geometry of 1 Kg TNT explosion

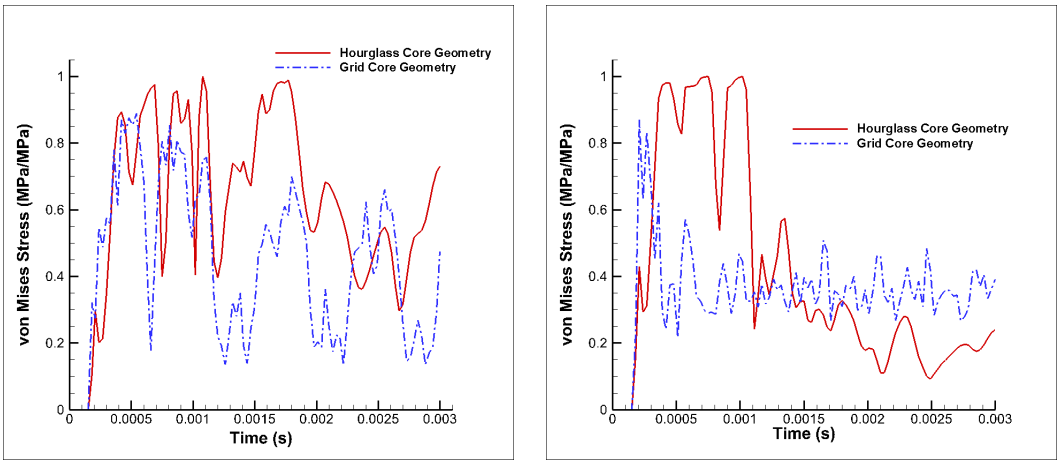

(a) With QP1180 (b) With S700MC and TRIP1180

Figure 4.22: Normalized von Mises Stress Comparison Graph in Core Geometry of 1 Kg TNT explosion

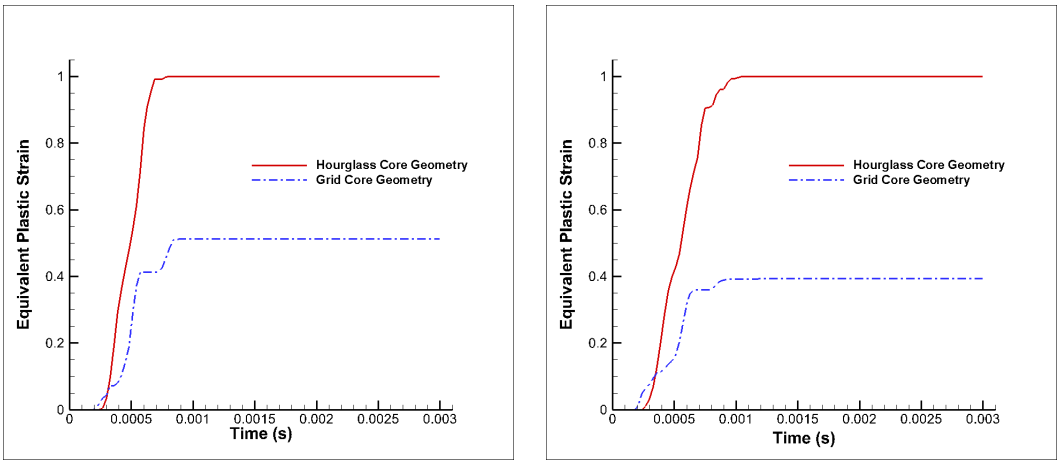

(a) With QP1180 (b) With S700MC and TRIP1180

Figure 4.23: Normalized Equivalent Plastic Strain Comparison Graph in Core Geometry of 3 Kg TNT explosion

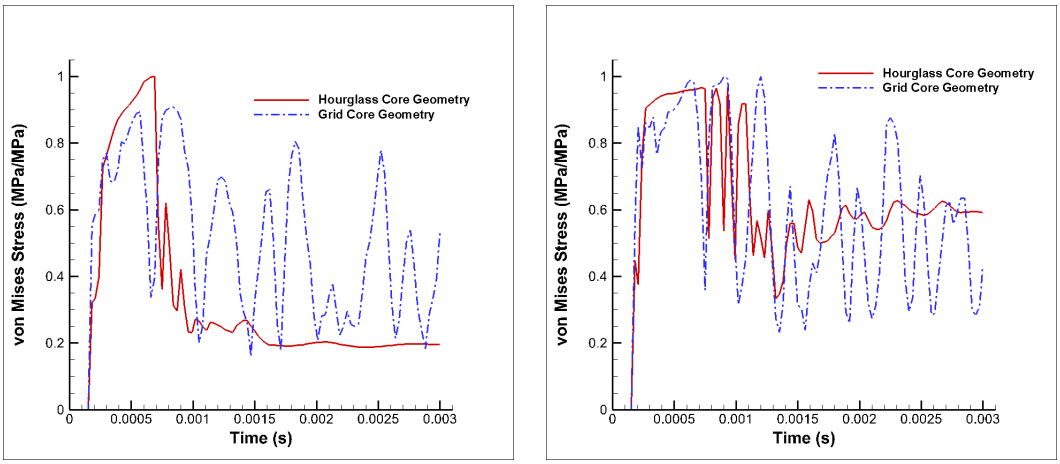

(a) With QP1180 (b) With S700MC and TRIP1180

Figure 4.24: Normalized von Mises Stress Comparison Graph in Core Geometry of 3 Kg TNT explosion

When the strain values under fixed boundary conditions are compared, since the grid core geometry is still quite stiff, the maximum von-Mises stress is observed at the edges rather than focal point, and the maximum strain value for 1 Kg and 3 Kg TNT explosion occurs in the region where the boundary conditions are defined. Figure 4.18 shows that equivalent plastic strain values approximately same which is 15%. Although, for hourglass core geometry, this value is observed at maximum displacement region, these values is observed at edge region for grid core geometry. This situation increases the possibility of failure at the connection points inside the vehicle in the grid core sandwich structure. Figure 4.20 shows us that there is a difference between the displacement values of the grid and hourglass core geometries. While the hourglass core structure was displaced by about 100 mm, the grid core structure was displaced by about 40 mm under 3 Kg TNT blast loads.

Although the equivalent plastic strain values in 1 Kg and 3 Kg TNT explosion are close in both geometries, the highest maximum displacement point is observed in the hourglass core geometry. This shows that the core structure performance is more desirable during the explosion. In addition, the values shown in Figure 4.21, Figure 4.22, Figure 4.23 and Figure 4.24 show that the core geometry of the hourglass structure absorbs more energy. For example, it is observed 7% equivalent plastic strain values for grid core geometry, but hourglass core geometry has 20% equivalent plastic strain values in core geometry under 3 Kg TNT blast loads. According to Figure4.24, von Mises stress values reaches approximately same values, which is 900 MPa, but for hourglass core geometry, stress value stabilizes more quickly under 3 Kg TNT blast load.

Figure 4.21 and Figure 4.23 show that the strain values of the hourglass structure are lower than the grid structure and the hourglass core structure undergoes more severe plastic deformation than the grid core structure. Grid core structure mainly deforms elastically. This shows that the energy transmitted from the source is absorbed within the core geometry for the hourglass structure. In the grid structure, the energy is less damped and transmitted to the upper plate. This is caused by the hourglass structure being topologically more prone to buckling.

CHAPTER 5

CONCLUSION AND DISCUSSION

In this thesis, as mentioned in the literature [7], sandwich structures, which are more advantageous in terms of energy absorption than monolith structures, and the behaviour of different core geometries against high impulse loading were investigated. Structures such as honeycomb geometry, which are widely used in the literature, were selected for reference analysis, and different core geometry types were also prepared for reference analysis. The optimum geometry was determined in the final analyses made with the selected geometries after the reference analysis. The hourglass core structure and the grid core structure used in the final analyses basically showed two different characteristics. During the study, convenience was taken into account in terms of production, rather than just a topology optimization. In addition, material optimization was not aimed, all analyses were made with fixed parameters. Desirable geometry was determined by considering ease of fabrication, von Mises stress and plastic strain values. It is determined that the hourglass core geometry is more effective than the grid core geometry. The displacement values obtained as a result of the analyses are within the desired limits. In addition, while creating the geometry, the mass/surface area ratio was kept within the limits. While reaching this result, the high energy absorption value of the hourglass core structure and the stiffer behaviour of the grid core structure were found to be the most important factors. It is observed that the shock wave transmitted from the source to the structure is more absorbed by more buckling core structure.

In the light of this information, further research can be conducted in order to investigate the performance of the mine-kit mounted a real armoured vehicle. Using the distribution of real armoured vehicle weights and the effect of gravity when defin-

ing boundary conditions will provide clearer results on the numerical analysis side and will provide realistic data for predicting the overall protective performance of the mine kit. In addition, further optimization can be made in the core structure geometry to increase the energy dissipation.

REFERENCES

[1] Presidency of Defence Industries: Turkish Defence Industry Product Catalogue, Internet:https://www.ssb.gov.tr/urunkatalog/en/10/, 2019 [April 22, 2021]

[2] FNSS Defence Systems Industry, "Product List", Internet:https://www.fnss.com.tr/en/products, 2021 [April 22, 2021]

[3] Faidzi,M.K.,Abdullah, S., Abdullah,M.F.,Azman,A.H.,Hui,D.,Singh,S.S.K., "Review of Current Trends for Metal Based Sandwich Panel: Failure Mechanisms and Their Contribution Factors" in *JEng.Failure Analysis*, 2021,pp. 105-302

[4] Ramnath, B. Vijaya, et al. "A Review on Sandwich Composites and Their Advancements" in *Materials Today: Proceedings*,vol. 16, 2019, pp. 1146-1151.

[5] Wang,Z.,"Recent Advantages in Novel Metallic Honeycomb Structure" in *Composites Part B: Engineering* ,2019, pp. 731-741.

[6] Belingardi,G.,Beyene,A.T.,Koricho,E.G.,Martorana,B.,"Alternative Lightweight Materials and Composites Manufacturing Technologies for Vehicle Frontal Bumper Beam" in *Composites Structures* vol. 120 ,2015, pp. 483-495.

[7] Hutchinson, J.W., Xue, Z., "Metal Sandwich Plates Optimized for Pressure Impulses" *Int. J. Mech. Sci.* vol. 47, 2005, pp. 545–569.

[8] Rahman,N.A.,Abdullah,S.,Abdullah,M.F.,Zamri,W.F.H.,Omar,M.Z.,Sajuri,Z., "Experimental and Numerical Investigation on the Layering Configuration Effect to the Laminated Aluminium/Steel Panel Subjected to High Speed Impact Test" in *Metals 8.9* ,2018, pp. 732.

[9] Abdullah,M.F.,Abdullah,S.,Omar,M.Z.,Sajuri,Z.,Risby,M.S.,"Observing the Behaviour of Reinforced Magnesium Alloy with Corbon-Nanotube and Lead Under 976 m/s Projectile Impact" in *J. Mech. Eng.* vol. 5 ,2018, pp. 129-141.

[10] Jamil, W.N.M. , Aripin,M.A. , Sajuri,Z., Abdullah, S., Omar, M.Z.,Abdullah,M.F. , Zamri,W.F.H. ,"Mechanical Properties and Microstructures of Steel Panels for Laminated Composites in Armoured Vehicles" in *Int.J.Automot.Mech.Eng.* ,2016, pp. 3742-3753.

[11] Xue, Z., Hutchinson, J.W.,"A Comparative Study of Impulse-Resistant Metal Sandwich Plates" *Int. J. Impact Eng.* vol. 30, 2004, pp. 1283–1305.

[12] Qin,Q.,Yuan,C.,Zhang,J.,Wang,T.J.,"Large Deflection Response of Rectangular Metal Sandwich Plates Subjected To Blast Loading" *Eur.J.Mech. A/Solids*, 2014, pp. 14-22

[13] Wang,Z.,Zhou,Y.,Wang,X.,Zhang,X.,"Multi-Objective Optimization Design of a Multi-Layer Honeycomb Sandwich Structure Under Blast Loading" *Proc.Institut. Mech.Engineers,Part D:J.Automobile Eng.*, 2017, pp. 1449-1458.

[14] Yazici,M.,Wright,J.,Bertin,D.,Shukla,A.,"Experimental and Numerical Study of Foam Filled Corrugated Core Steel Sandwich Structures Subjected to Blast Loading" *Compos. Struct.*, 2014, pp. 98-109.

[15] Deshpande, V.S., Fleck, N.A.,"One-Dimensional Response Shock Response of Sandwich Plates" *J. Mech. Phys. Solids 53*, 2005, pp. 2347-2383.

[16] Fleck, N.A.,Deshpande, V.S., "The Resistance of Clamped Sandwich Beams to Shock Loading" in *J. Appl. Mech.*, 2004, pp. 386-401.

[17] Qiu,X.,Despande,V.S.,Fleck,N.A.,"Finite Element Analysis of the Dynamic Response of Clamped Sandwich Beams" *Eur.J.Mech.A/Solids*, 2003, pp. 801-814.

[18] Tilbrook, M.T., Deshpande, V.S., Fleck, N.A.,"The Impulsive Response of Sandwich Beams: Analytical and Numerical Investigation of Regimes of Behavior" *J. Mech. Phys. Solids 54*, 2006, pp. 2242–2280.

[19] Dharmasena, K.P., Wadley, H.N.G., Xue, Z., Hutchinson., J.W.,"Mechanical Response of Metallic Honeycomb Sandwich Panel Structures to High-Intensity Dynamic Loading" *Int. J. Impact Eng.*, 2007, pp. 1063-1074.

[20] Xue, Z., Hutchinson, J.W.,"Crush Dynamics of Square Honeycomb Sandwich Cores" *Int. J. Num. Method Eng. 65*, 2006, pp. 2221–2245.

[21] AEP-55, Volume 2 (Edition 2), "Procedures for Evaluating the Protection Level of Armoured Vehicles: Mine Threat" *NATO Allied Engineering Publication* , 2011.

[22] North Atlantic Treaty Organization, "STANAG 4569, Protection Levels For Occupants of Armored Vehicles", Jan. 2004

[23] Sadek,E.A.,"Dynamic Optimisation of a Sandwich Beam" *Comput. Struct.*, 1984, pp. 605-615.

[24] Johnson,A.F.,Sims,S.D.,"Mechanical Properties and Design of Sandwich Beams" *Composites*, 1986, pp. 321-328.

[25] Gibson,L.J.,"Optimisation of Stiffness in Sandwich Beams with Rigid Foam Cores" *Mater. Sci. Eng.*, 1984, pp. 125-135.

[26] Gordaninejad,F.,Bert,C.W.,"A New Theory for Bending of Thick Sandwich Beams" *Int. J. Mech. Sci.*, 1989, pp. 925-934.

[27] Jones, N., "A Theoretical Study of the Dynamic Plastic Behaviour of Beams and Plates With Finite Deflection" *Int. J. Solid Struct. 7*, 1971, pp. 1007-1029.

[28] Symmonds, P.S., "Large Plastic Deformations of Beams Under Blast Type Loading" *Proceedings of the Second U.S. National Congress of Applied Mechanics*, 1954, pp. 505-515.

[29] Taylor, G.I., "The Pressure and Impulse of Submarine Explosion Waves on Plates" *The Scientific Papers of G.I. Taylor, Vol III, Cambridge Univ. Press*, 1963, pp. 287-303.

[30] Cole, R.H., "Underwater Explosion" *Princeton University Press*, 1948.

[31] Swisdak,M.M., "Explosion Effects and Properties-Part II:Explosion Effects in Water" *Technical Report, Naval Surface Weapons Center*, 1978.

[32] Erdik, A.,Kılıç, N.,Bedir, S.,Ak, H., "Mayın Patlama Simülasyonlarında Üç Farklı Yöntemin İncelenmesi: CONWEP, MM-ALE ve Birleşik CONWEP-ALE" *SAVTEK 2014 Savunma Teknolojileri Kongresi*, 2014

[33] Mazurkiewicz, L., Malachowski,J.,Baranowski,P.,Damaziak,K.,"Comparison of Numerical Testing Methods in Terms of Impulse Loading Applied to Structural Elementes" *Journal of Theoretical and Applied Mechanics*, 2013, pp. 615-625.

[34] C.N. Kinger, G.Bulmash, "Airblast parameters from TNT Spherical Air Burst and Hemispherical Surface Burst", Report ARBL-TR-02555, U.S. BRL, Aberdeen Proving Ground MD,1984

[35] Johnson, G.R.,Cook, W.H., "A Constitutive Model and Data for Metals Subjected to Large Strains, High Strain Rates and High Temperatures" *Proceedings of the 7th International Symposium on Ballistic*, 1983, pp. 541-547.